Statistical mechanics of nanotubes

Siddhartha Sarkar,[1, 2, *] Mohamed El Hedi Bahri,[2, †] and Andrej Košmrlj[2, 3, ‡]

[1]*Department of Physics, University of Michigan, Ann Arbor, MI 48109, USA*
[2]*Department of Mechanical and Aerospace Engineering,*
Princeton University, Princeton, NJ 08544, USA
[3]*Princeton Institute for the Science and Technology of Materials,*
Princeton University, Princeton, NJ 08544, USA

We investigate the effect of thermal fluctuations on the mechanical properties of nanotubes by employing tools from statistical physics. For 2D sheets it was previously shown that thermal fluctuations effectively renormalize elastic moduli beyond a characteristic temperature-dependent thermal length scale (a few nanometers for graphene at room temperature), where the bending rigidity increases, while the in-plane elastic moduli reduce in a scale-dependent fashion with universal power law exponents. However, the curvature of nanotubes produces new phenomena. In nanotubes, competition between stretching and bending costs associated with radial fluctuations introduces a characteristic elastic length scale, which is proportional to the geometric mean of the radius and effective thickness. Beyond elastic length scale, we find that the in-plane elastic moduli stop renormalizing in the axial direction, while they continue to renormalize in the circumferential direction beyond the elastic length scale albeit with different universal exponents. The bending rigidity, however, stops renormalizing in the circumferential direction at the elastic length scale. These results were verified using molecular dynamics simulations.

I. INTRODUCTION

Atomically thin membranes have been a subject of interest over the last few decades [1–5] for their promising electronic and mechanical properties. Thin solid membranes are also ubiquitous in soft condensed matter [6–8] and biological systems [9–17]. In these contexts, the statistical mechanics of freely suspended elastic membranes have been studied extensively [18–31]. Theoretical studies of these membranes suggest that due to long-range interaction between local Gaussian curvatures mediated by in-plane phonons, arbitrarily large elastic membranes can remain flat at low enough temperatures [18–23]. In such membranes, the thermal fluctuations stiffen the bending rigidity κ in a scale (ℓ) dependent fashion, $\kappa(\ell) \sim \ell^\eta$, and reduce the Young's modulus $Y(\ell) \sim \ell^{-\eta_u}$ beyond a temperature T dependent length $\ell_{\rm th} \sim \sqrt{\kappa_0^2/(k_B T Y_0)}$, where κ_0 and Y_0 are the microscopic bending rigidity and Young's modulus respectively. This result has been obtained using various methods such as perturbative renormalization group with ϵ-expansion [22, 24, 25], $1/d$-expansion [23], self consistent screening approximation [26, 27] and nonperturbative renormalization group [28–30], verified with numerical simulations [32–34], and being studied in experiments [35].

Atomically thin cylindrical shell-like structures are important in the context of carbon nanotubes. Since its invention in 1991 [2], carbon nanotubes have gained significant research interest due to their electronic properties [36], high tensile strength [37, 38], thermal conductivity [38] and their ability to adsorb gases [39]. They have been used in field-effect transistors [40], composite materials [41], environmental monitoring [39] etc. For these applications, it is important to study the effect of thermal fluctuations on the mechanical properties of nanotubes. While thermal fluctuations of flat sheets are well understood, much less is known about the response of nanotubes to thermal fluctuations.

Here we investigate the statistical mechanics of thin single-walled nanotubes at low temperatures within shallow shell approximation [42–44]. Due to the presence of the curvature in nanotubes, the radial fluctuations along the axial direction cost both bending and stretching energy, whereas the radial fluctuations along the circumferential direction only cost bending energy. This competition between stretching and bending costs associated with height fluctuations introduces a characteristic elastic length scale ($\ell_{\rm el} \sim \sqrt{Rt}$) [45, 46], which is proportional to the geometric mean of the radius and effective thickness. In typical carbon naotubes, this length is $\ell_{\rm el} \lesssim 3$nm. We show that below this length, the bending rigidity and in-plane moduli scales the same way as for flat membranes mentioned above. As will be discussed in detail in this article, beyond the elastic length scale, the in-plane elastic moduli stop renormalizing in the axial direction, while they continue to renormalize in the circumferential direction beyond the elastic length scale

---

albeit with different universal exponents. The bending rigidity, however, stops renormalizing in the circumferential direction at the elastic length scale. We verify our theoretical findings with molecular dynamics simulations.

The remainder of the paper is organized as follows. In Sec. II, we review shallow shell theory description for cylindrical shells. In Sec. III, we set up the statistical mechanics problem. In Sec. IV, we perform renormalization group and scaling analysis to show how the elastic moduli scale in different regimes. In Sec. V, we compare the theoretically predictions with molecular dynamics simulations. In Sec. VI, we give concluding remarks and comment on possible further investigations for better understanding of the mechanical properties of thermalized cylindrical shells.

II. ELASTIC ENERGY OF DEFORMATION

The elastic energy of a deformed cylindrical shell can be estimated with shallow shell theory. To this end, let us consider a cylindrical shell with radius R and length L in its undeformed configuration. [47] Then, any point on the undeformed shell can be written as $\bar{\mathbf{X}} = (R\cos\varphi, R\sin\varphi, z)$ in cartesian coordinates where the axis of the cylinder is in the z direction. Since the radius R is a constant, the shell can be parametrized by $(R\varphi, z)$ coordinates. The tangent vectors at any point on the shell can be written as $\bar{\mathbf{t}}_\varphi = \partial_\varphi \bar{\mathbf{X}} = (-\sin\varphi, \cos\varphi, 0)$ and $\bar{\mathbf{t}}_z = \partial_z \bar{\mathbf{X}} = (0, 0, 1)$, whereas the normal is $\bar{\mathbf{N}} = (\cos\varphi, \sin\varphi, 0)$. Note that here we used short-hand $\partial_\varphi \equiv \frac{1}{R}\frac{\partial}{\partial\varphi}$ and $\partial_z \equiv \frac{\partial}{\partial z}$. The reference metric is $\bar{g}_{ij} = \bar{\mathbf{t}}_i \cdot \bar{\mathbf{t}}_j = \delta_{ij}$ and curvature tensor is $\bar{b}_{ij} = \bar{\mathbf{N}} \cdot \partial_i \bar{\mathbf{t}}_j = -\frac{1}{R}\delta_{ij}\delta_{i\varphi}$ where $i \in \{\phi, z\}$. Then, in the deformed configuration, the displacement of each point can be decomposed into tangential components $u_i(R\varphi, z)$ (where $i \in \{\varphi, z\}$) and radial component $h(R\varphi, z)$ (see Fig. 1(a)) such that the coordinates of the points in deformed configuration are given by $\mathbf{X} = \bar{\mathbf{X}} + \mathbf{u}_\varphi \bar{\mathbf{t}}_\varphi + \mathbf{u}_z \bar{\mathbf{t}}_z + h\bar{\mathbf{N}}$. The tangent vectors in the deformed configuration are $\mathbf{t}_\varphi = \partial_\varphi \mathbf{X} = \bar{\mathbf{t}}_\varphi + \bar{\mathbf{t}}_\varphi \partial_\varphi u_\varphi - \frac{1}{R}u_\varphi \bar{\mathbf{N}} + \bar{\mathbf{t}}_z \partial_\varphi u_z + \bar{\mathbf{N}}\partial_\varphi h + \frac{1}{R}h\bar{\mathbf{t}}_\varphi$ and $\mathbf{t}_z = \partial_z \bar{\mathbf{X}} = \bar{\mathbf{t}}_z + \bar{\mathbf{t}}_\varphi \partial_z \mathbf{u}_\varphi + \bar{\mathbf{t}}_z \partial_z \mathbf{u}_z + \bar{\mathbf{N}}\partial_z h$. Then, the metric and the curvature tensors in the deformed configuration are:

$$g_{ij} \approx \delta_{ij} + \partial_i u_j + \partial_j u_i + (\partial_i h)(\partial_j h) + \frac{2}{R}h\delta_{ij}\delta_{i\varphi},$$
$$b_{ij} \approx -\frac{1}{R}\delta_{ij}\delta_{i\varphi} + \partial_i\partial_j h, \tag{1}$$

where we kept only the relevant terms (in the sense of Wilsonian renormalization [48]) in displacements and their derivatives. This is termed as the Donnell-Mushtari-Vlasov approximation [42–44]. The in-plane strain and bending strain tensors are defined as $u_{ij} \equiv (g_{ij} - \bar{g}_{ij})/2$ and $K_{ij} \equiv (b_{ij} - \bar{b}_{ij})$, respectively [42]. Then, from Eq. 1, we find

$$u_{ij} = (\partial_i u_j + \partial_j u_i + \partial_i h \partial_j h)/2 + \frac{h}{R}\delta_{ij}\delta_{i\varphi},$$
$$K_{ij} = \partial_i\partial_j h, \tag{2}$$

where $i, j \in \{\varphi, z\}$. Notice that first term inside the parenthesis in the expression of in-plane strain u_{ij} is the same as in flat sheets. However, the second term is not present for flat sheets and will couple in-plane strains with the radial undulation field h due to curvature $1/R$. The free energy cost of the shell deformation is given by:

$$F = \int_A dA \frac{1}{2}\left[\kappa_0(K_{ii})^2 + \lambda_0(u_{ii})^2 + 2\mu_0(u_{ij})^2\right], \tag{3}$$

where the first term accounts for the bending energy and the last two terms are the in-plane stretching energy. Note that we did not consider the term consisting of the Gaussian curvature because we are interested in studying the system under periodic boundary conditions, where the integral of the Gaussian curvature is zero due to the Gauss-Bonnet theorem. Here, κ_0 is the microscopic (bare) bending rigidity of the material and has dimensions of energy, whereas λ_0 and μ_0 are the microscopic (bare) Lamé coefficients and has the dimension of energy per area and $dA = d\varphi dz R$ is the infinitesimal area element with $A = 2\pi RL$ being the area of the system. We furthermore define ds as the infinitesimal line element at the boundary, ∂A is the boundary of the cylinder, $\mathbf{T}$ is the traction force at the boundary. The components of the traction force can be written as $T_i = n_j\sigma_{ij}$ where σ_{ij} is the homogeneous stress tensor and n_j is the in-plane normal to at the boundary. Replacing this expression of the traction force T_i and using Stokes' theorem we get:

$$\int_{\partial A} ds\, T_i u_i = \int_{\partial A} ds\, n_j\sigma_{ij}u_i = \int_A dA \partial_j(\sigma_{ij}u_i) = \int_A dA \sigma_{ij}\partial_j u_i = \sigma_{ij}\int_A dA \frac{1}{2}(\partial_j u_i + \partial_i u_j),$$
$$F = \int_A dA \frac{1}{2}\left[\kappa_0(\nabla^2 h)^2 + \lambda_0(u_{ii})^2 + 2\mu_0(u_{ij})^2 - \sigma_{ij}(\partial_j u_i + \partial_i u_j)\right], \tag{4}$$
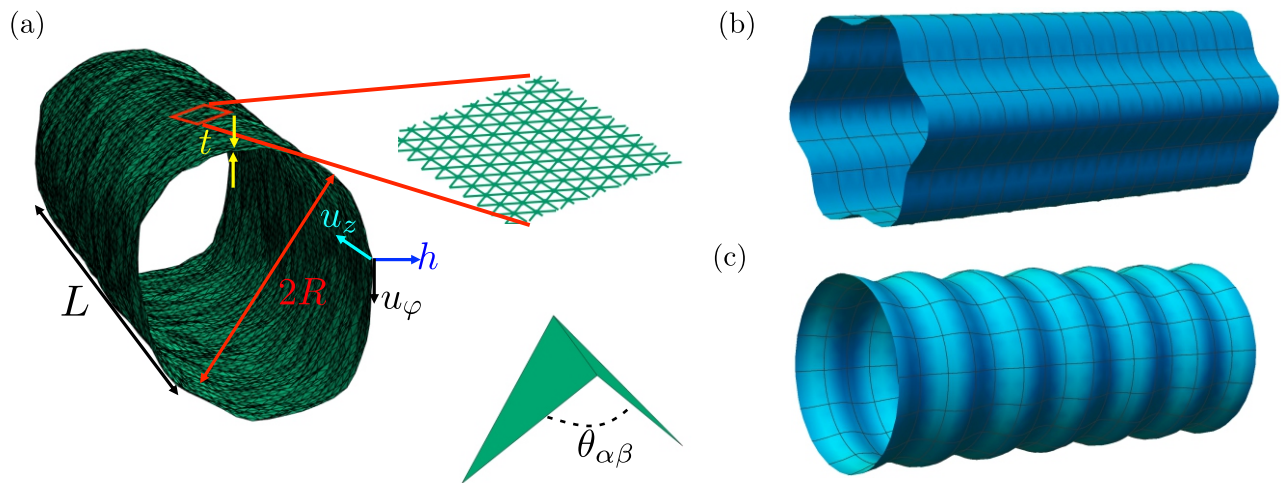
FIG. 1. (a) A snaphot of a thermally fluctuating cylindrical shell. The length L, diameter $2R$, thickness t, in-plane displacements u_φ and u_z, radial displacement h are shown. A small segment (shown in red box) on the shell is zoomed in to show that in simulations, the shell is modeled with triangular lattice of point masses connected by harmonic springs (green lines). At bottom right corner, the angle $\theta_{\alpha\beta}$ between two adjacent triangles of the triangular lattice is shown. (b) A deformed cylindrical shell with only nonzero $\tilde{h}(q_\varphi \neq 0, q_z = 0)$ and $\tilde{h}(q_\varphi = 0, q_z = 0)$ does not cost stretching energy if the change in the length of circumference due to $\tilde{h}(q_\varphi \neq 0, q_z = 0)$ is compensated by $\tilde{h}(q_\varphi = 0, q_z = 0)$. (c) A deformed cylindrical shell with nonzero $\tilde{h}(q_\varphi = 0, q_z \neq 0)$ and $\tilde{h}(q_\varphi = 0, q_z = 0)$ costs stretching energy different positions along the axis of the cylindrical shell have different circumference length.

where we used the facts that $\sigma_{ij} = \sigma_{ji}$ and $K_{ii} = \nabla^2 h$. We also assume that the microscopic material is isotropic which is reasonable for carbon nanotubes. However, inspection of the last term in the expression of u_{ij} in Eq. 2 shows that it is anisotropic. This means that as we integrate small wavelength degrees of freedom to investigate long wavelength behavior, the moduli may become anisotropic. Keeping this in mind, we write the more general form of the free energy is given below:

$$F = \int_A dA \, \frac{1}{2} \left[B^0_{ijkl}(\partial_i \partial_j h)(\partial_k \partial_l h) + C^0_{ijkl} u_{ij} u_{kl} - \sigma_{ij}(\partial_j u_i + \partial_i u_j) \right], \tag{5}$$

where B^0_{ijkl} and C^0_{ijkl} are the most general bare bending rigidity and in-plane elastic tensors, respectively. However, because of the mirror planes $x - y$ and $r - z$, the anisotropy can be at most orthorhombic, meaning that $B_{\varphi\varphi\varphi z} = B_{\varphi z z z} = C_{\varphi\varphi\varphi z} = C_{\varphi z z z} = 0$. This along with the major and minor symmetries of B_{ijkl} and C_{ijkl} tensors mean that the only independent moduli are $B_{\varphi\varphi\varphi\varphi}$, $B_{\varphi\varphi z z}$, B_{zzzz}, $C_{\varphi\varphi\varphi\varphi}$, $C_{\varphi\varphi z z}$, $C_{\varphi z \varphi z}$ and C_{zzzz}. For isotropic bare rigidities, $B^0_{ijkl} = \kappa_0 \delta_{ij} \delta_{kl}$ and $C^0_{ijkl} = \lambda_0 \delta_{ij} \delta_{kl} + \mu_0 (\delta_{ik} \delta_{jl} + \delta_{il} \delta_{jk})$.

III. THERMAL FLUCTUATIONS

The effect of thermal fluctuations can be seen in the correlation functions obtained from the functional integrals:

$$\langle h \rangle \equiv \langle h(\mathbf{x}) \rangle = \frac{1}{Z} \int \mathcal{D}[u_i, h] h(\mathbf{x}) e^{-F/k_B T}, \tag{6a}$$

$$G_{hh}(\mathbf{x}_2 - \mathbf{x}_1) \equiv \langle \delta h(\mathbf{x}_2) \delta h(\mathbf{x}_1) \rangle = \frac{1}{Z} \int \mathcal{D}[u_i, h] \delta h(\mathbf{x}_2) \delta h(\mathbf{x}_1) e^{-F/k_B T}, \tag{6b}$$

$$G_{u_i u_j}(\mathbf{x}_2 - \mathbf{x}_1) \equiv \langle u_i(\mathbf{x}_2) u_j(\mathbf{x}_1) \rangle = \frac{1}{Z} \int \mathcal{D}[u_i, h] u_i(\mathbf{x}_2) u_j(\mathbf{x}_1) e^{-F/k_B T}, \tag{6c}$$

$$Z = \int \mathcal{D}[u_i, h] e^{-F/k_B T}, \tag{6d}$$

where T is the temperature, k_B is the Boltzmann's constant, Z is the partition function, $\delta h(\mathbf{x}) = h(\mathbf{x}) - \langle h \rangle$, $\mathbf{x} \equiv (R\varphi, z)$, and in Eqs. 6a, 6b and 6c, we used the fact the system is translationally invariant.

In the following, we decompose the radial displacement field as $h(\mathbf{x}) = h_0 + \tilde{h}(\mathbf{x})$, where $h_0 = (1/A)\int dA\, h(\mathbf{x})$ is the homogeneous part of the undulation field, and $(1/A)\int dA\, \tilde{h}(\mathbf{x}) = 0$. Then, $\langle h_0 \rangle = (1/A)\int dA \langle h(\mathbf{x}) \rangle = \langle h \rangle$. With this knowledge then, $\delta h(\mathbf{x}) = \tilde{h}(\mathbf{x}) + h_0 - \langle h_0 \rangle$. Similarly, the in-plane strain fields can be decomposed into $u_{ij}(\mathbf{x}) = u_{ij}^0 + \tilde{u}_{ij}(\mathbf{x})$. However, the homogeneous strain $u_{\varphi\varphi}^0$ and the zero mode of the radial fluctuation h_0 are related by $u_{\varphi\varphi}^0 = h_0/R$ because increasing the length in azimuthal direction effectively increases the radius. Integrating out the homogeneous fields h_0 and u_{ij}^0, we obtain the following effective free energy:

$$
\begin{aligned}
F_{\text{eff},1} &= -k_B T \ln\left(\int \mathcal{D}[u_{\varphi z}^0, h_0, u_{zz}^0] e^{-F/k_B T}\right) \\
&= \int_A dA\, \frac{1}{2}\left[B_{ijkl}^0 (\partial_i \partial_j \tilde{h})(\partial_k \partial_l \tilde{h}) + C_{ijkl}^0 \tilde{u}_{ij}\tilde{u}_{kl} + \sigma_{ij}(\partial_i \tilde{h})(\partial_j \tilde{h})\right] \\
&= F_0 + F_I, \\
F_0/A &= \int_A dA\, \frac{1}{2}\left[B_{ijkl}^0 (\partial_i \partial_j \tilde{h})(\partial_k \partial_l \tilde{h}) + \frac{C_{\varphi\varphi\varphi\varphi}^0}{R^2}\tilde{h}^2 + \sigma_{ij}(\partial_i \tilde{h})(\partial_j \tilde{h})\right] \\
&\quad + \int_A dA\, \frac{1}{2}\left[C_{ijkl}^0 (\partial_i \tilde{u}_j)(\partial_k \tilde{u}_l) + C_{ij\varphi\varphi}^0 (\partial_i \tilde{u}_j)\frac{\tilde{h}}{R}\right], \\
F_I/A &= \int_A dA\, \frac{1}{2}\left[C_{ijkl}^0 \partial_i \tilde{u}_j (\partial_k \tilde{h})(\partial_l \tilde{h}) + C_{\varphi kl}^0 \frac{\tilde{h}}{R}(\partial_k \tilde{h})(\partial_l \tilde{h})\right] \\
&\quad + \int_A dA\, \frac{1}{8}C_{ijkl}^0 (\partial_i \tilde{h})(\partial_j \tilde{h})(\partial_k \tilde{h})(\partial_l \tilde{h}),
\end{aligned} \tag{7}
$$

where F_0 and F_I are the harmonic and anharmonic parts of the effective free energy $F_{\text{eff},1}$. A similar functional integral shows that the average radial and axial extensions are:

$$\frac{\langle h \rangle}{R} = \frac{\langle h_0 \rangle}{R} = \frac{\sigma_{\varphi\varphi}}{Y_{\varphi\varphi}^0} - \frac{\nu_{\varphi\varphi}^0 \sigma_{zz}}{Y_{\varphi\varphi}^0} - \frac{1}{2}\langle(\partial_\varphi \tilde{h})^2\rangle, \tag{8a}$$

$$\frac{\langle \Delta L \rangle}{L} = \langle u_{zz}^0 \rangle = \frac{\sigma_{zz}}{Y_{zz}^0} - \frac{\nu_{zz}^0 \sigma_{\varphi\varphi}}{Y_{zz}^0} - \frac{1}{2}\langle(\partial_z \tilde{h})^2\rangle, \tag{8b}$$

where $Y_{\varphi\varphi}^0 = C_{\varphi\varphi\varphi\varphi} - C_{\varphi\varphi zz}^2/C_{zzzz}$ and $Y_{zz}^0 = C_{zzzz} - C_{\varphi\varphi zz}^2/C_{\varphi\varphi\varphi\varphi}$ are the 2-dimensional Young's moduli in the azimuthal and axial directions respectively, and $\nu_{\varphi\varphi} = C_{\varphi\varphi zz}/C_{zzzz}$ and $\nu_{zz} = C_{\varphi\varphi zz}/C_{\varphi\varphi\varphi\varphi}$ are the Poisson's ratios in azimuthal and axial directions respectively. For isotropic microscopic properties, $Y_{\varphi\varphi}^0 = Y_{zz}^0 = 4\mu_0(\lambda_0 + \mu_0)/(\lambda_0 + 2\mu_0) \equiv Y_0$, and $\nu_{\varphi\varphi}^0 = \nu_{zz}^0 = \lambda_0/(\lambda_0 + 2\mu_0) \equiv \nu_{\text{iso}}^0$. The last terms in Eqs. 8a and 8b are negative meaning that in absence of any normal stress ($\sigma_{\varphi\varphi} = \sigma_{zz} = 0$), the radius and the length of the cylindrical shell shrink under thermal fluctuations. This is because nonuniform radial fluctuations $\tilde{h}(\mathbf{x})$ at fixed radius would increase the integrated area, with a large stretching energy cost. The system prefers to wrinkle and shrink its radius to gain entropy while keeping the integrated area of the convoluted shell approximately constant.

For renormalization group calculations, it is sometimes helpful to integrate out the in-plane phonons and write an

effective free energy as a functional of radial undulations:

$$F_{\text{eff}} = -k_B T \ln \left(\int \mathcal{D}[u_\varphi, u_z] e^{-F_{\text{eff},1}/k_B T} \right) = F_{\text{eff}}^0 + F_{\text{eff}}^I,$$

$$F_{\text{eff}}^0/A = \sum_{\mathbf{q} \neq \mathbf{0}} \frac{1}{2} \left[B_{ijkl}^0 q_i q_j q_k q_l + \frac{N(C_{ijkl}^0) q_z^4}{R^2 D(C_{ijkl}^0; \mathbf{q})} + \sigma_{ij} q_i q_j \right] \tilde{h}(\mathbf{q}) \tilde{h}(-\mathbf{q}),$$

$$F_{\text{eff}}^I/A = \sum_{\mathbf{q}_1 + \mathbf{q}_2 = -\mathbf{q} \neq \mathbf{0}} \frac{q_z^2}{2q^2} [q_{1i} P_{ij}^T(\mathbf{q}) q_{2j}] \frac{N(C_{ijkl}^0) q^4}{RD(C_{ijkl}^0; \mathbf{q})} \tilde{h}(\mathbf{q}) \tilde{h}(\mathbf{q}_1) \tilde{h}(\mathbf{q}_2)$$

$$+ \sum_{\substack{\mathbf{q}_1 + \mathbf{q}_2 = \mathbf{q} \neq \mathbf{0} \\ \mathbf{q}_3 + \mathbf{q}_4 = -\mathbf{q} \neq \mathbf{0}}} \frac{1}{8} [q_{1i} P_{ij}^T(\mathbf{q}) q_{2j}][q_{3i} P_{ij}^T(\mathbf{q}) q_{4j}] \frac{N(C_{ijkl}^0) q^4}{D(C_{ijkl}^0; \mathbf{q})} \tilde{h}(\mathbf{q}_1) \tilde{h}(\mathbf{q}_2) \tilde{h}(\mathbf{q}_3) \tilde{h}(\mathbf{q}_4), \quad (9)$$

$$N(C_{ijkl}) = \det(C_{ijkl})/4 = C_{\varphi\varphi\varphi\varphi} C_{\varphi z\varphi z} C_{zzzz} - C_{\varphi\varphi zz}^2 C_{\varphi z\varphi z},$$

$$D(C_{ijkl}; \mathbf{q}) = \det(C_{kilj} q_k q_l) = \frac{1}{2} (\varepsilon_{i_1 i_2} \varepsilon_{j_1 j_2} C_{k_1 i_1 l_1 j_1} C_{k_2 i_2 l_2 j_2} q_{k_1} q_{k_2} q_{l_1} q_{l_2})$$

$$= C_{\varphi\varphi\varphi\varphi} C_{\varphi z\varphi z} q_\varphi^4 + (C_{\varphi\varphi\varphi\varphi} C_{zzzz} - 2C_{\varphi\varphi zz} C_{\varphi z\varphi z} - C_{\varphi\varphi zz}^2) q_\varphi^2 q_z^2$$

$$+ C_{zzzz} C_{\varphi z\varphi z} q_z^4,$$

where $P_{ij}^T(\mathbf{q}) = (\delta_{ij} - q_i q_j/q^2)$, ε_{ij} is the permutation symbol, and we took Fourier transform of the radial undulation field $\tilde{h}(\mathbf{q}) = \int_A (dA/A) h(\mathbf{x}) e^{-i\mathbf{q} \cdot \mathbf{x}}$. Note that in the isotropic case, $Nq^4/D(C_{ijkl}^0; \mathbf{q}) = Y_0$. Note that F_{eff}^0 and F_{eff}^I are the harmonic and anharmonic part of the effective free energy F_{eff}. Then, within harmonic approximation one can read off the Fourier transform $G_{hh}^0(\mathbf{q}) = \int_A (dA/A) G_{hh}^0(\mathbf{x}) e^{-i\mathbf{q} \cdot \mathbf{x}}$ of the correlation function $G_{hh}^0(\mathbf{x})$ (the superscript "0" is for harmonic approximation):

$$G_{hh}^0(\mathbf{q}) \equiv \langle |\tilde{h}(\mathbf{q})|^2 \rangle_0 = \frac{k_B T/A}{B_{ijkl}^0 q_i q_j q_k q_l + \frac{N(C_{ijkl}^0) q_z^4}{R^2 D(C_{ijkl}^0; \mathbf{q})} + \sigma_{ij} q_i q_j} \overset{\text{isotropic}}{=} \frac{k_B T/A}{\kappa_0 q^4 + \frac{Y_0 q_z^4}{R^2 q^4} + \sigma_{ij} q_i q_j}, \quad (10)$$

where $\langle \rangle_0$ is the harmonic average. The effect of the anharmonic terms is to replace the bare parameters B_{ijkl}^0, C_{ijkl}^0 and σ_{ij} with scale dependent renormalized parameters $B_{ijkl}^R(\mathbf{q})$, $C_{ijkl}^R(\mathbf{q})$ and $\sigma_{ij}^R(\mathbf{q})$:

$$G_{hh}(\mathbf{q}) \equiv \langle |\tilde{h}(\mathbf{q})|^2 \rangle = \frac{k_B T/A}{B_{ijkl}^R(\mathbf{q}) q_i q_j q_k q_l + \frac{N(C_{ijkl}^R(\mathbf{q})) q_z^4}{R^2 D(C_{ijkl}^R(\mathbf{q}); \mathbf{q})} + \sigma_{ij}^R(\mathbf{q}) q_i q_j}. \quad (11)$$

Before going into the details of renormalization, it is useful to gain some insights from the Green's function in Eq. 10. In the limit $R \to \infty$, it gives back the Green's function for isotropic sheets $G_{hh}^{s,0}(\mathbf{q}) = \frac{k_B T/A}{\kappa_0 q^4 + \sigma_{ij} q_i q_j}$. Because of the presence of anisotropic curvature in the cylindrical shell, we have, in the denominator, an extra direction dependent term $(Y_0 q_z^4)/(R^2 q^4)$ which suppresses the amplitude of the radial fluctuations in the axial direction. This because the Fourier modes of radial fluctuations which are in axial direction necessarily cost stretching energy along with bending energy, whereas the Fourier modes of radial fluctuations which are in azimuthal direction only cost bending energy (see Fig. 1(b) and (c)) [46]. Furthermore, setting external stresses to zero $\sigma_{ij} = 0$ and equating the two remaining terms in the denominator of Eq. 10, we obtain a characteristic wave vector:

$$q_{\text{el}}^0 \equiv \frac{\pi}{\ell_{\text{el}}^0} = \left(\frac{Y_0}{\kappa_0 R^2} \right)^{\frac{1}{4}} = \frac{\gamma^{\frac{1}{4}}}{R}, \quad (12)$$

where $\gamma = Y_0 R^2/\kappa_0$ is the Föppl-von Karman number. In the theory of shallow shells, $\kappa_0 \sim Et^3$ and $Y_0 \sim Et$, where E is 3-dimensional Young's modulus of the material and t is the thickness of shell. In atomically thin systems thickness is not well defined; however, we can define an effective thickness as $t \sim \sqrt{\kappa_0/Y_0}$ Then, the Föppl-von Karman number $\gamma \sim R^2/t^2$ meaning that the larger γ is, the larger the radius R is with respect to the thickness t. The length scale ℓ_{el}^0 obtained from this is what we will call the "elastic length scale." The superscript "0" is for harmonic approximation; we will see later that when we take renormalization of the parameters due to the anharmonic terms into account, the expression of ℓ_{el} changes slightly. As we will see in the next section, the effect of the curvature on the renormalization of the material parameters is negligible for scales smaller the elastic length scale ℓ_{el} and will be

important at scales larger than this. Another important length scale that is important for both isotropic sheets and cylindrical shells comes from the form of the Green's function: $G_{hh}^0 \sim \frac{k_B T}{A \kappa_0 q^4}$ when $\sigma_{ij} = 0$ and $q \gg q_{\text{el}}^0$. Therefore, the largest amplitude of the radial (height in case of sheets) fluctuations occur when $q \sim 1/L$ and $A \sim L^2$ (where is the system size) giving largest amplitude of the radial fluctuation as $h_{\text{th}} \sim L\sqrt{k_B T/\kappa_0} = L\tau^{1/2}$ ($\tau \equiv k_B T/\kappa_0$ is the nondimensional temperature). Anharmonic terms become important when this amplitude is of the order of the thickness $h_{\text{th}} \sim t \sim \sqrt{\kappa_0/Y_0}$. This gives us a length $\ell_{\text{th}} \sim \sqrt{\kappa_0^2/(k_B T Y_0)}$ called thermal length scale [49] (we will get a better estimate of ℓ_{th} later in Eq. 20). The effect of the anharmonic terms are only important when the system size is larger than the thermal length scale ℓ_{th}. These two length scales ℓ_{th} and ℓ_{el} divides the scale dependence of the material parameters into three regimes. We will be interested in the limit where $\ell_{\text{th}} \ll \ell_{\text{el}}$ because as was discussed above, below ℓ_{th} the anharmonic terms are not important and thus the theory is trivial. Therefore, keeping this length smaller than other important length scales enables us to see all possible non-trivial scalings due to the anharmonic terms. In addition, we will be interested in zero external stress limit $\sigma_{ij}^R(q) = 0$.

IV.   RENORMALIZATION GROUP AND SCALING ANALYSIS

The effect of the anharmonic terms in Eq. 7 at a given scale $\ell^* \equiv \pi/q^*$ can be obtained by systematically integrating out all degrees of freedom on smaller scales (i.e., larger wave vectors). This can be done by splitting the displacement fields into pieces: $g_<(\mathbf{r}) = \sum_{|\mathbf{q}|<q^*} e^{i\mathbf{q}\cdot\mathbf{r}} g(\mathbf{q})$ and $g_>(\mathbf{r}) = \sum_{\Lambda>|\mathbf{q}|>q^*} e^{i\mathbf{q}\cdot\mathbf{r}} g(\mathbf{q})$, where $g \in \{\tilde{u}_i, \tilde{h}\}$ and $a \equiv \pi/\Lambda$ is a microscopic cutoff, and integrating out $g_>$ as

$$
\begin{aligned}
F_{\text{eff},1}(\ell^*) &= -k_B T \ln\left(\int \mathcal{D}[\tilde{u}_{i,>}, \tilde{h}_>] e^{-F_{\text{eff},1}/k_B T}\right), \\
F_{\text{eff}}(\ell^*) &= -k_B T \ln\left(\int \mathcal{D}[\tilde{h}_>] e^{-F_{\text{eff},1}/k_B T}\right).
\end{aligned}
\tag{13}
$$

A.   Scaling analysis for $\ell^* \ll \ell_{\text{el}}$

- $\ell^* \ll \ell_{\text{th}} \ll \ell_{\text{el}}^0$: we have $C_{\varphi\varphi\varphi\varphi}^0 |\tilde{h}(\mathbf{q})|^2/R^2 \ll \kappa_0(q^*)^4 |\tilde{h}(\mathbf{q})|^2$, meaning that we can ignore the term $C_{\varphi\varphi\varphi\varphi}^0 \tilde{h}^2/R^2$ from Eq. 7, and similarly we can ignore the term $N(C_{ijkl}^0)q_z^4/(R^2 D(C_{ijkl}^0;\mathbf{q}))\tilde{h}(\mathbf{q})\tilde{h}(-\mathbf{q}) \sim Y_0 q_z^4/(R^2 q^4)\tilde{h}(\mathbf{q})\tilde{h}(-\mathbf{q})$ from Eq. 9. Since $\ell^* \ll \ell_{\text{th}}$, the anharmonic terms are not important as was discussed in the last section. Therefore, the effective harmonic free energy is

$$
F_{\text{eff}}(\ell^*) = \sum_{\substack{\mathbf{q}\neq\mathbf{0} \\ q<q^*}} \frac{A}{2}\left[B_{ijkl}^0 q_i q_j q_k q_l + \sigma_{ij} q_i q_j\right] = \sum_{\substack{\mathbf{q}\neq\mathbf{0} \\ q<q^*}} \frac{A}{2}\left[\kappa_0 q^4 + \sigma_{ij} q_i q_j\right]\tilde{h}(\mathbf{q})\tilde{h}(-\mathbf{q}).
\tag{14}
$$

This free energy is isotropic and the material parameters remain the same as their bare values. The naïve (Gaussian or harmonic) dimensions of the quantities $\tilde{h}(\mathbf{q})$ and σ_{ij} requiring that $[F_{\text{eff}}] = 0$ and $[\kappa_0] = 0$ and expressing dimensionality in wave-vector units [50]:

$$
[\tilde{h}(\mathbf{q})] = -1 = (D-4)/2 \equiv -\zeta_h, [\sigma_{ij}] = 2,
\tag{15}
$$

where $D = 2$ is the dimension of the system. The meaning of these dimensions is that under the scale transformation $\mathbf{q} \to \mathbf{q}' = b\mathbf{q}$ or $\mathbf{x} \to \mathbf{x}' = b^{-1}\mathbf{x}$, if we transform $\tilde{h}(\mathbf{q}) \to \tilde{h}'(\mathbf{q}') = b^{[\tilde{h}(\mathbf{q})]}\tilde{h}(b\mathbf{q}) = b^{-1}\tilde{h}(b\mathbf{q})$ and $\sigma_{ij} \to \sigma_{ij}' = b^{[\sigma_{ij}]}\sigma_{ij} = b^2\sigma_{ij}$, the harmonic theory remains invariant. With these dimensions we go back to $F_{\text{eff},1}$ in Eq. 7 and find the naïve dimensions of the following quantities:

$$
[C_{ijkl}^0] = 2 = 4 - D, [\tilde{u}_i] = -1 = D - 3 = 1 - 2\zeta_h, [1/R] = 1 = D/2.
\tag{16}
$$

This means that under scale transformation $\mathbf{q} \to \mathbf{q}' = b\mathbf{q}$, $C_{ijkl}'^0 = b^{4-D}C_{ijkl}^0$ meaning as we zoom out of the system $C_{ijkl}'^0$ grows for dimensions $D < 4$. Since C_{ijkl}^0 are the coefficients of the anharmonic terms in Eq. 7, the anharmonic terms are important for dimensions $D \leq 4$. This implies that the upper critical dimension of the theory in Eq. 7 is $D_u = 4$ and the anharmonic terms are relevant in the physical dimension $D = 2$. This means that the anharmonic terms will renormalize the parameters B_{ijkl}^0 and C_{ijkl}^0 at least in the regime $\ell_{\text{th}} < \ell^* \ll \ell_{\text{el}}^0$ which we discuss next.

- $\ell_{\rm th} < \ell^* \ll \ell^0_{\rm el}$: In this regime, the anharmonic renormalize the parameters B^0_{ijkl} and C^0_{ijkl} to parameters $B^R_{ijkl}(\mathbf{q}^*)$ and $C^R_{ijkl}(\mathbf{q}^*)$ at scale q^*. However, for $\ell^* \gtrsim \ell_{\rm th}$ when the parameters are only mildly renormalized, the anisotropic term $N^R(\mathbf{q})q_z^4/(R^2 D^R(\mathbf{q}))$ in the denominator of the Green's function in Eq. 11 is still small w.r.t. the first term $B^R_{ijkl}(\mathbf{q})q_iq_jq_kq_l$(we will show the consistency of this once we obtain the renormalization group flow equations). Therefore, we can implement an isotropic (circular) momentum-shell renormalization group scheme. We first integrate out all Fourier modes in a thin momentum shell $\Lambda/b < q < \Lambda$ and $b \equiv \ell^*/a = e^s$, with $s \ll 1$. Next we rescale lengths and fields:

$$\mathbf{r} = b\mathbf{r}', \ \tilde{h}(\mathbf{r}) = b^{\zeta_h}\tilde{h}(\mathbf{r}'), \ \tilde{u}_i(\mathbf{r}) = b^{2\zeta_h-1}\tilde{u}_i(\mathbf{r}') \tag{17}$$

where ζ_h is the field-rescaling exponent. We find it convenient to work directly with a $D = 2$-dimensional cylindrical shell embedded in $d = 3$ space, rather than introducing an expansion in $\epsilon = 4 - D$ [22, 24]. In principle, this is dangerous and can give wrong results because if we work in $D = 2$, $\epsilon = 4 - 2 = 2$ is large and there is no small parameter in the perturbative renormalization scheme. However, later we show using the molecular dynamics simulations that the results obtained by directly working in $D = 2$ matches with simulations. Finally, we define new elastic moduli B'_{ijkl}, C'_{ijkl}, and a new external pressure σ'_{ij}, such that the free-energy functional in Eqs. 7 and 9 retain the same form after the renormalization group steps. We then write the ordinary differential equations for the parameters w.r.t. s, called β functions [50, 51]. To obtain the contribution to the renormalization of B_{ijkl} from the anharmonic terms, we find it easier to work with the effective free energy $F_{\rm eff}$ where the in-plane phonon are completely integrated out (see Fig. 2). However, for C_{ijkl}, it is much simpler to use the free energy $F_{\rm eff,1}$ (see Fig. 3). To one-loop order we get:
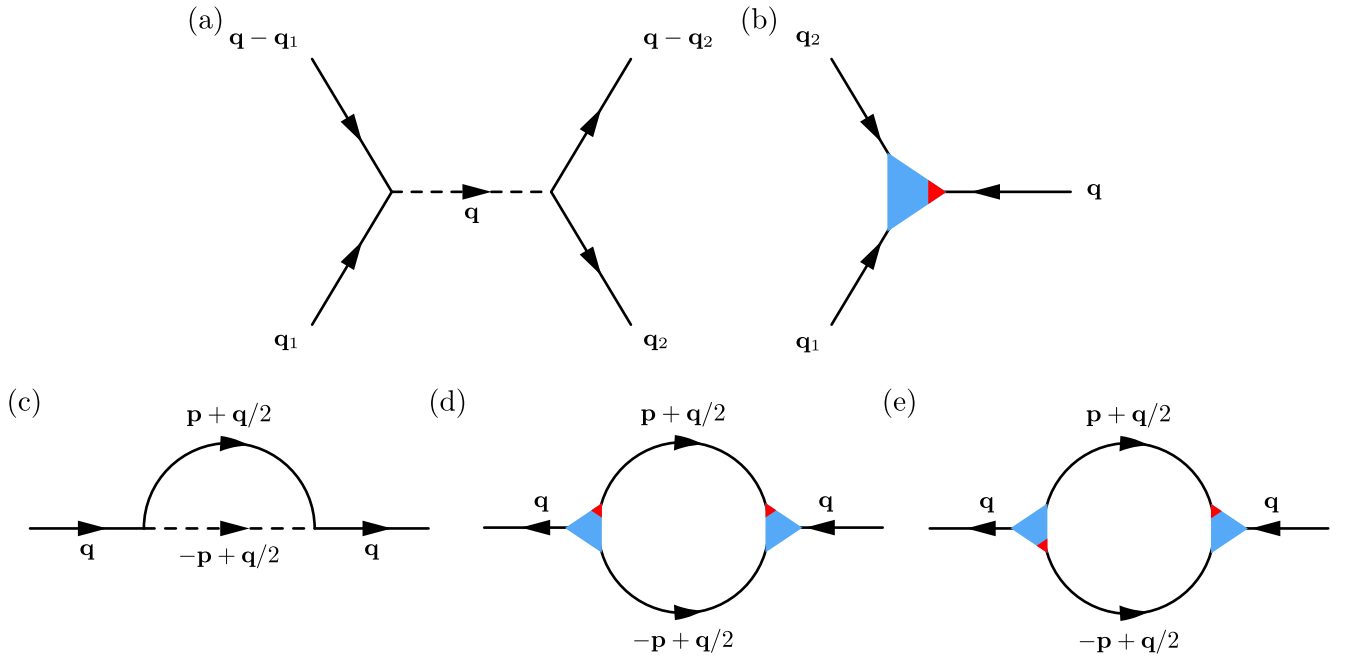

FIG. 2. Feynman diagrams relevant to the renormalization of bending rigidity. (a) Four-point and (b) three-point vertices describe the quartic and cubic terms in the effective free energy of Eq. 9, respectively. the straight legs represent radial displacement fields $\tilde{h}(\mathbf{q})$. The red part of the three-point vertex in (b) connects to the field $\tilde{h}(\mathbf{q})$ corresponding to wave vector which is in the argument of P^T_{ij}. (c–e) One-loop diagrams that contribute to the renormalization flows of the bending rigidities B^R_{ijkl}. The momentum $\mathbf{p}$ in (c), (d), (e) is the loop momentum which is integrated over a shell $\Lambda/b < p < \Lambda$ and whole Fourier space in momentum-shell renormalization and self consistent calculation respectively.

$$\beta_{B_{ijkl}} = \frac{dB'_{ijkl}}{ds} = 2(\zeta_h - 1)B'_{ijkl} + \frac{A}{4\pi^2}\frac{d}{ds}\int_{\Lambda/b<|\mathbf{p}|<\Lambda} d^2\mathbf{p}\, \varepsilon_{im}\varepsilon_{jn}\varepsilon_{kr}\varepsilon_{lt}p_mp_np_rp_t\frac{N(C'_{ijkl})}{D(C'_{ijkl};\mathbf{p})}G_{hh}(\mathbf{p})$$

$$- \frac{2A^2}{4\pi^2 R'^2 k_B T}\frac{d}{ds}\int_{\Lambda/b<|\mathbf{p}|<\Lambda} d^2\mathbf{p}\, \varepsilon_{im}\varepsilon_{jn}\varepsilon_{kr}\varepsilon_{lt}p_mp_np_rp_tp_z^4\frac{N^2(C'_{ijkl})}{D^2(C'_{ijkl};\mathbf{p})}G^2_{hh}(\mathbf{p}), \tag{18a}$$
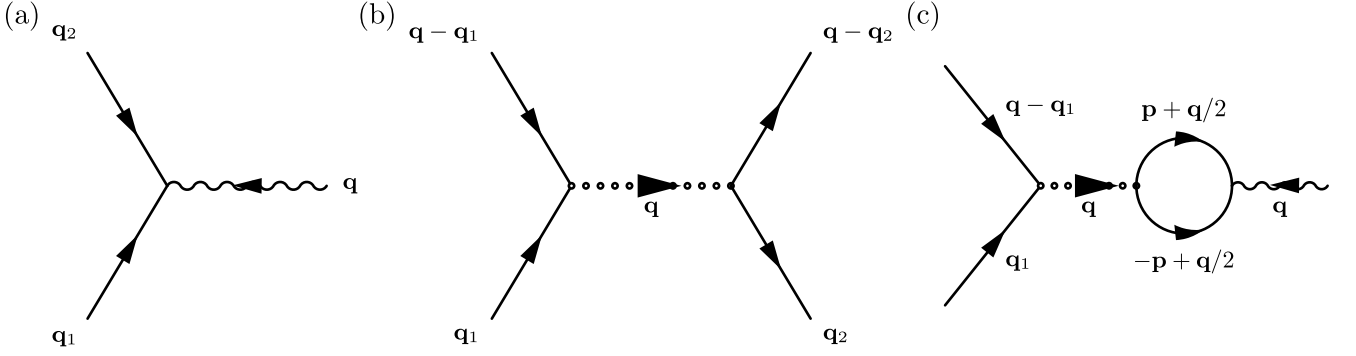
FIG. 3. Feynman diagrams relevant to the renormalization of in-plane moduli. (a) Three-point (b) four-point vertices describe the cubic $\tilde{u}h\tilde{h}$ and quartic $\tilde{h}\tilde{h}\tilde{h}\tilde{h}$ terms in the free energy of Eq. 7, respectively. The wiggly line in (a) is the leg correspoding to in-plane displacement field $\tilde{u}_i(\mathbf{q})$. (c) One-loop diagram that contributes to the renormalization flows of the in-plane stiffnesses C_{ijkl}^R associated with the three-point vertex in (a). The connected legs in these diagrams represent the propagators $G_{hh}(\mathbf{q})$. The momentum $\mathbf{p}$ in (c) is the loop momentum which is integrated over a shell $\Lambda/b < p < \Lambda$ and whole Fourier space in momentum-shell renormalization and self consistent calculation respectively.

$$\beta_{C_{ijkl}} = \frac{dC'_{ijkl}}{ds} = 2(2\zeta_h - 1)C'_{ijkl} - \frac{A^2}{8\pi^2 k_B T}C'_{ijmn}C'_{rtkl}\frac{d}{ds}\int_{\Lambda/b<|\mathbf{p}|<\Lambda} d^2\mathbf{p}\, p_m p_n p_r p_t G_{hh}^2(\mathbf{p}), \tag{18b}$$

$$\beta_{\sigma_{ij}} = \frac{d\sigma'_{ij}}{ds} = 2\zeta_h \sigma'_{ij}, \tag{18c}$$

$$\beta_R = \frac{dR'}{ds} = -R', \tag{18d}$$

where ε_{ij} is the permutation symbol ($\varepsilon_{11} = \varepsilon_{22} = 0$ and $\varepsilon_{12} = -\varepsilon_{21} = 1$). The scale-dependent parameters B'_{ijkl}, C'_{ijkl}, and σ'_{ij}, obtained by integrating the differential equations in Eqs. 18 up to a scale $s = \ln(\ell^*/a)$ with initial conditions $B'_{ijkl}(0) = \kappa_0\delta_{ij}\delta_{kl}$, $C_{ijkl}(0) = \lambda_0\delta_{ij}\delta_{kl} + \mu_0(\delta_{ik}\delta_{jl} + \delta_{il}\delta_{jk})$ and $\sigma_{ij}(0) = 0$, are related to the scale-dependent renormalized parameters as $B_{ijkl}^R(s) = B'_{ijkl}(s)e^{(2-2\zeta_h)s} = B'_{ijkl}(s)$, $C_{ijkl}^R(s) = C'_{ijkl}(s)e^{(2-4\zeta_h)s} = C'_{ijkl}(s)e^{-2s}$ and $\sigma_{ij}^R(s) = \sigma'_{ij}(s)e^{-2s}$, since $\zeta_h = 1$.

With the initial conditions just mentioned, the only term that can make the RG flow anisotropic is the last term in Eq. 18a. In the limit $\ell_{th} < \ell^* \ll \ell_{el}^0$, the second and third terms in Eq. 18a are $\sim k_B T Y'/(\kappa'\Lambda^2)$ and $\sim k_B T Y'^2/(\kappa'^2 R'^2\Lambda^6)$ respectively. The third term is of the order of the second terms when:

$$k_B T Y'/(\kappa'\Lambda^2) \lesssim k_B T Y'^2/(\kappa'^2 R'^2\Lambda^6)$$
$$\Rightarrow k_B T Y_R(s)e^{2s}a^2/\kappa_R(s) \lesssim k_B T Y_R^2(s)e^{4s}a^6/(\kappa_R^2(s)R^2 e^{-2s})$$
$$\Rightarrow 1 \lesssim Y_R(s)(\ell/a)^4 a^4/(\kappa_R(s)R^2)$$
$$\Rightarrow \ell \gtrsim (\kappa_R(s)R^2/Y_R(s))^{1/4} \tag{19}$$

Comparing the right hand side of the last line of Eq. 19 with Eq. 12, we define a new elastic length scale as

$$\ell_{el} \equiv \frac{\pi}{q_{el}} = \pi\left(\frac{\kappa_R(\ell_{el})R^2}{Y_R(\ell_{el})}\right)^{\frac{1}{4}}, \tag{20}$$

where $\kappa_R(\ell_{el})$ and $Y_R(\ell_{el})$ are themselves dependent on the elastic length scale. We will give a better estimate of elastic length later. From, Eq. 19, we see that the third term in Eq. 18a, which is anisotropic, is negligible compared to the isotropic second term in the regime $\ell_{th} < \ell^* \ll \ell_{el}$, and can be ignored. Therefore, in this region the material parameters remain isotropic. In this limit, the β-functions are exactly the same as those for a thermally fluctuating isotropic sheet [49]. Hence, in this regime, the scale dependence of the isotropic material parameters is the same as in case of isotropic sheets:

$$\frac{\kappa_R(\ell)}{\kappa_0} \approx (\ell/\ell_{th})^\eta, \ell_{th} \ll \ell \ll \ell_{el},$$

$$\frac{\lambda_R(\ell)}{Y_0}, \frac{\mu_R(\ell)}{Y_0}, \frac{Y_R(\ell)}{Y_0} \approx c(\ell/\ell_{th})^{-\eta_u}, \ell_{th} \ll \ell \ll \ell_{el}, \tag{21}$$

where the prefactor c is -0.36, 0.72 and 1.0 for λ_R, μ_R and Y_R respectively [49], $\eta \approx 0.8 - 0.85$ [26, 28, 49], and the exponents η and η_u satisfy the identity $2\eta + \eta_u = 2$, which is a result of infinitesimal rotational symmetry of the system about in-plane axes [22]. Replacing These expressions of $\kappa_R(\ell)$ and $Y_R(\ell)$ in Eq. 20 we get the following estimate of elastic length:

$$\ell_{\rm el} = \frac{\pi}{q_{\rm el}} = \left(\frac{\kappa_0 R^2 q_{\rm th}^{\eta+\eta_u}}{Y_0} \right)^{\frac{1}{4-\eta-\eta_u}}. \tag{22}$$

A better estimate of the thermal length scale can also be obtained from Eq. 18a. This is the scale, $\ell = ae^s$, at which the second term is comparable to the first (Gaussian) term of Eq. 18a is the system size where the anharmonicity of the free energy becomes important. Then, by simplifying the second term in Eq. 18a using the fact that the material parameters are isotropic and using the expressions $\kappa'(s) = \kappa_R(s) \approx \kappa_0$ (the last equality is due to the fact that the parameters only start to renormalize at the thermal length scale), $Y'(s) = Y_R(s)e^{2s} \approx Y_0 e^{2s} \approx \kappa_0(s)$, $s = \ln(\ell_{\rm th}/a)$, $\Lambda = \pi/a$, we get [49]:

$$\ell_{\rm th} \equiv \frac{\pi}{q_{\rm th}} = \sqrt{\frac{16\pi^3 \kappa_0^2}{3k_B T Y_0}}. \tag{23}$$

B. Scaling analysis for $\ell^* \gg \ell_{\rm el}$

Thus far, in our discussion, we have seen that up to the elastic length scale the parameters remain isotropic and $B_{ijkl}^R(q_{\rm el}) \approx \kappa_R(q_{\rm el})\delta_{ij}\delta_{kl} \approx \delta_{ij}\delta_{kl}\kappa_0(q_{\rm el}/q_{\rm th})^{-\eta}$ and $C_{ijkl}^R(q_{\rm el}) \approx \lambda_R(q_{\rm el})\delta_{ij}\delta_{kl} + \mu_R(q_{\rm el})(\delta_{ik}\delta_{jl} + \delta_{il}\delta_{jk}) \approx Y_0(-0.36\delta_{ij}\delta_{kl} + 0.72(\delta_{ik}\delta_{jl} + \delta_{il}\delta_{jk}))(q_{\rm el}/q_{\rm th})^{\eta_u}$. Therefore, integrating out the degrees of freedom on scales smaller than $\ell_{\rm el}$, the free energy takes the form:

$$
\begin{aligned}
F_{\rm eff}^0(q_{\rm el})/A &= \sum_{\substack{\mathbf{q}\neq 0 \\ q<q_{\rm el}}} \frac{1}{2}\left(B_{ijkl}^R(q_{\rm el})q_i q_j q_k q_l + \frac{q_z^4 N(C_{ijkl}^R(q_{\rm el}))}{R^2 D(C_{ijkl}^R(q_{\rm el}); \mathbf{q})} \right) \tilde{h}(\mathbf{q})\tilde{h}(-\mathbf{q}) \\
&\approx \sum_{\substack{\mathbf{q}\neq 0 \\ q<q_{\rm el}}} \frac{1}{2}\left(\kappa_R(q_{\rm el})q^4 + \frac{q_z^4 Y_R(q_{\rm el})}{R^2 q^4} \right) \tilde{h}(\mathbf{q})\tilde{h}(-\mathbf{q}),
\end{aligned} \tag{24a}
$$

$$
\begin{aligned}
F_{\rm eff}^I(q_{\rm el})/A &= \sum_{\substack{\mathbf{q}_1+\mathbf{q}_2=-\mathbf{q}\neq 0 \\ q_1,q_2,q<q_{\rm el}}} \frac{q_z^2}{2q^2}[q_{1i}P_{ij}^T(\mathbf{q})q_{2j}] \frac{N(C_{ijkl}^R(q_{\rm el}))q^4}{RD(C_{ijkl}^R(q_{\rm el}); \mathbf{q})} \tilde{h}(\mathbf{q})\tilde{h}(\mathbf{q}_1)\tilde{h}(\mathbf{q}_2) \\
&\quad + \sum_{\substack{\mathbf{q}_1+\mathbf{q}_2=\mathbf{q}\neq 0 \\ \mathbf{q}_3+\mathbf{q}_4=-\mathbf{q}\neq 0 \\ q_1,q_2,q_3,q_4,q<q_{\rm el}}} \frac{1}{8}[q_{1i}P_{ij}^T(\mathbf{q})q_{2j}][q_{3i}P_{ij}^T(\mathbf{q})q_{4j}] \frac{N(C_{ijkl}^R(q_{\rm el}))q^4}{D(C_{ijkl}^R(q_{\rm el}); \mathbf{q})} \tilde{h}(\mathbf{q}_1)\tilde{h}(\mathbf{q}_2)\tilde{h}(\mathbf{q}_3)\tilde{h}(\mathbf{q}_4), \\
&\approx \sum_{\substack{\mathbf{q}_1+\mathbf{q}_2=-\mathbf{q}\neq 0 \\ q_1,q_2,q<q_{\rm el}}} [q_{1i}P_{ij}^T(\mathbf{q})q_{2j}] \frac{Y_R(q_{\rm el})q_z^2}{2Rq^2} \tilde{h}(\mathbf{q})\tilde{h}(\mathbf{q}_1)\tilde{h}(\mathbf{q}_2) \\
&\quad + \sum_{\substack{\mathbf{q}_1+\mathbf{q}_2=\mathbf{q}\neq 0 \\ \mathbf{q}_3+\mathbf{q}_4=-\mathbf{q}\neq 0 \\ q_1,q_2,q_3,q_4,q<q_{\rm el}}} \frac{Y_R(q_{\rm el})}{8}[q_{1i}P_{ij}^T(\mathbf{q})q_{2j}][q_{3i}P_{ij}^T(\mathbf{q})q_{4j}] \tilde{h}(\mathbf{q}_1)\tilde{h}(\mathbf{q}_2)\tilde{h}(\mathbf{q}_3)\tilde{h}(\mathbf{q}_4).
\end{aligned} \tag{24b}
$$

Starting from this course-grained free energy, the harmonic approximation to the Green's function is:

$$G_{hh}^0(\mathbf{q}; q < q_{\rm el}) = \frac{k_B T/A}{\kappa_R(q_{\rm el})q^4 + \frac{Y_R(q_{\rm el})q_z^4}{R^2 q^4}}, \tag{25}$$

which is aniosotropic for $q < q_{\rm el}$. Now, following the argument of [52] (section V), the regime of wavevectors that dominates the $\tilde{h}$-fluctuations is $q^8 \approx (q_{\rm el}q_z)^4$ i.e., $q_z = q_\varphi^2/q_{\rm el}$. Therefore, for small $q \ll q_{\rm el}$, $q_z \sim q_\varphi^2 \ll q_\varphi$. This leads

to a simplification of the expression of $D(C_{ijkl}; \mathbf{q})$ keeping only the lowest order terms in q_φ:

$$\frac{q_z^4 N(C_{ijkl}^R(q_{\mathrm{el}}))}{D(C_{ijkl}^R(q_{\mathrm{el}}); \mathbf{q})} \approx \frac{C_{\varphi\varphi\varphi\varphi}^R(q_{\mathrm{el}})C_{\varphi z\varphi z}^R(q_{\mathrm{el}})C_{zzzz}^R(q_{\mathrm{el}}) - C_{\varphi\varphi zz}^R(q_{\mathrm{el}})^2 C_{\varphi z\varphi z}^R(q_{\mathrm{el}})}{C_{\varphi\varphi\varphi\varphi}^R(q_{\mathrm{el}})C_{\varphi z\varphi z}^R(q_{\mathrm{el}})} \frac{q_z^4}{q_\varphi^4} = Y_{zz}^R(q_{\mathrm{el}})\frac{q_z^4}{q_\varphi^4}. \tag{26}$$

In this regime, if we count the dimension of wave vector component q_φ as $[q_\varphi] = 1$, we have to count the dimension of q_z as $[q_z] = 2$ since $q_z \sim q_\varphi^2$. This happens in strongly anisotropic systems, see for example [53]. In fact the scaling theory that will be presented in this paper is identical to that of tubules found in [52] as well as that of membranes under uni-axially tension [54]. Though these are different systems physically, the scaling of the correlation functions and the arguments to obtain these scalings are identical. Then, the dimension of area A is $[A] = -1 - 2 = -3$. With these, and requiring that Gaussian part of the effective free energy

$$F_{\mathrm{eff}}^0(q_{\mathrm{el}}) \approx \sum_{\substack{\mathbf{q} \neq 0 \\ q < q_{\mathrm{el}}}} \frac{A}{2} \left(B_{ijkl}^R(q_{\mathrm{el}})q_i q_j q_k q_l + \frac{q_z^4 Y_{zz}^R(q_{\mathrm{el}})}{R^2 q_\varphi^4} \right) \tilde{h}(\mathbf{q})\tilde{h}(-\mathbf{q}) \tag{27}$$

dimensionless, we get the following naïve dimensions:

$$[\tilde{h}(\mathbf{q})] = -1/2, [B_{\varphi\varphi\varphi\varphi}^R(q_{\mathrm{el}})] = 0, [B_{\varphi\varphi zz}^R(q_{\mathrm{el}})] = -2, [B_{zzzz}^R(q_{\mathrm{el}})] = -4, [Y_{zz}^R(q_{\mathrm{el}})/R^2] = 0 \tag{28}$$

Therefore, the terms $B_{\varphi\varphi zz}^R(q_{\mathrm{el}})q_\varphi^2 q_z^2 \tilde{h}(\mathbf{q})\tilde{h}(-\mathbf{q})$, $B_{zzzz}^R(q_{\mathrm{el}})q_z^4 \tilde{h}(\mathbf{q})\tilde{h}(-\mathbf{q})$ are irrelevant. Keeping only the relevant terms then the harmonic part of the free energy is:

$$F_{\mathrm{eff}}^0(q_{\mathrm{el}}) \approx \sum_{\substack{\mathbf{q} \neq 0 \\ q < q_{\mathrm{el}}}} \frac{A}{2} \left(B_{\varphi\varphi\varphi\varphi}^R(q_{\mathrm{el}})q_\varphi^4 + \frac{q_z^4 Y_{zz}^R(q_{\mathrm{el}})}{R^2 q_\varphi^4} \right) \tilde{h}(\mathbf{q})\tilde{h}(-\mathbf{q}), \tag{29}$$

and the harmonic Green's function can be approximated as:

$$G_{hh}^0(\mathbf{q}; q < q_{\mathrm{el}}) \approx \frac{k_B T/A}{B_{\varphi\varphi\varphi\varphi}^R(q_{\mathrm{el}})q_\varphi^4 + \frac{Y_{zz}^R(q_{\mathrm{el}})q_z^4}{R^2 q_\varphi^4}}. \tag{30}$$

To get the naïve dimensions of other moduli, first go back to the form of the in-plane strain tensor and require that all the terms in the same component of strain have the same dimension. This way we get:

$$\begin{aligned}
\tilde{u}_{\varphi\varphi} &: [\partial_\varphi \tilde{u}_\varphi] = [\tilde{h}/R] = [(\partial_\varphi \tilde{h})^2] = 1 \Rightarrow [\tilde{u}_\varphi] = 0, [1/R] = 3/2, \\
\tilde{u}_{zz} &: [\partial_z \tilde{u}_z] = [(\partial_z \tilde{h})^2] = 3 \Rightarrow [\tilde{u}_z] = 1, \\
\tilde{u}_{\varphi z} &: [\partial_\varphi \tilde{u}_z] = [\partial_z \tilde{u}_\varphi] = [(\partial_z \tilde{h})(\partial_\varphi \tilde{h})] = 2,
\end{aligned} \tag{31}$$

where we used $\tilde{u}_{\varphi\varphi}$ and $\tilde{u}_{zz}$ get the dimensions of $\tilde{u}_\varphi$, $\tilde{u}_z$ and $1/R$, and checked their consistency with $\tilde{u}_{\varphi z}$. With these dimensions, we use the free energy in Eq. 7 to find the dimensions of $C_{ijkl}^R(q_{\mathrm{el}})$:

$$[C_{\varphi\varphi\varphi\varphi}^R(q_{\mathrm{el}})] = 1, [C_{\varphi\varphi zz}^R(q_{\mathrm{el}})] = [C_{\varphi z\varphi z}^R(q_{\mathrm{el}})] = -1, [C_{zzzz}^R(q_{\mathrm{el}})] = -3. \tag{32}$$

This means that only terms with $C_{\varphi\varphi\varphi\varphi}^R(q_{\mathrm{el}})$ as coefficient are relevant. Keeping only terms with coefficients $C_{\varphi\varphi\varphi\varphi}^R(q_{\mathrm{el}})$ in Eq. 7, if we integrate out the in-plane displacements, the interacting part $F_{\mathrm{eff}}^I(q_{\mathrm{el}})$ of effective free energy is $F_{\mathrm{eff}}^I(q_{\mathrm{el}}) = 0$. Therefore, the effective free energy:

$$F_{\mathrm{eff}}(q_{\mathrm{el}}) \approx F_{\mathrm{eff}}^0(q_{\mathrm{el}}) \approx \sum_{\substack{\mathbf{q} \neq 0 \\ q < q_{\mathrm{el}}}} \frac{A}{2} \left(B_{\varphi\varphi\varphi\varphi}^R(q_{\mathrm{el}})q_\varphi^4 + \frac{q_z^4 Y_{zz}^R(q_{\mathrm{el}})}{R^2 q_\varphi^4} \right) \tilde{h}(\mathbf{q})\tilde{h}(-\mathbf{q}) \tag{33}$$

describes a free field theory and $B_{\varphi\varphi\varphi\varphi}^R(q_{\mathrm{el}})$ and $Y_{zz}^R(q_{\mathrm{el}})$ do not renormalize any further as we integrate out Fourier modes beyond $q < q_{\mathrm{el}}$:

$$B_{\varphi\varphi\varphi\varphi}^R(\mathbf{q}) \approx B_{\varphi\varphi\varphi\varphi}^R(q_{\mathrm{el}}) = \kappa_R(q_{\mathrm{el}}) \approx \kappa_0(q_{\mathrm{el}}/q_{\mathrm{th}})^{-\eta}, \tag{34a}$$

$$Y_{zz}^R(\mathbf{q}) \approx Y_{zz}^R(q_{\mathrm{el}}) = Y_R(q_{\mathrm{el}}) \approx Y_0(q_{\mathrm{el}}/q_{\mathrm{th}})^{\eta_u}. \tag{34b}$$

Hence, the Green's function $G_{hh}(\mathbf{q}; q < q_{\text{el}}) = G_{hh}^0(\mathbf{q}; q < q_{\text{el}})$. However, the free energy in Eq. 7 is not a free field theory because $C_{\varphi\varphi\varphi\varphi}^R(q_{\text{el}})$ is relevant. Then we can use the Feynman diagram in Fig. 4 to write a self consistent perturbative equation (see a similar analysis in [52], see also [54] for more details):

$$C_{\varphi\varphi\varphi\varphi}^R(\mathbf{q}) = C_{\varphi\varphi\varphi\varphi}^R(q_{\text{el}}) - \frac{A^2}{8\pi^2 k_B T} (C_{\varphi\varphi\varphi\varphi}^R(\mathbf{q}) C_{\varphi\varphi\varphi\varphi}^R(q_{\text{el}})) \int_{|\mathbf{p}| < q_{\text{el}}} dp_\varphi dp_z \, p_\varphi^2 (p_\varphi - q_\varphi)^2 G_{hh}(\mathbf{p}) G_{hh}(\mathbf{p} - \mathbf{q})$$

$$= C_{\varphi\varphi\varphi\varphi}^R(q_{\text{el}}) - \frac{k_B T}{8\pi^2} (C_{\varphi\varphi\varphi\varphi}^R(\mathbf{q}) C_{\varphi\varphi\varphi\varphi}^R(q_{\text{el}})) \int_{|\mathbf{p}| < q_{\text{el}}} dp_\varphi dp_z \, p_\varphi^2 (p_\varphi - q_\varphi)^2 \times \tag{35}$$

$$\frac{1}{\left(B_{\varphi\varphi\varphi\varphi}^R(q_{\text{el}}) p_\varphi^4 + \frac{Y_{zz}^R(q_{\text{el}}) p_z^4}{R^2 p_\varphi^4}\right) \left(B_{\varphi\varphi\varphi\varphi}^R(q_{\text{el}})(p_\varphi - q_\varphi)^4 + \frac{Y_{zz}^R(q_{\text{el}})(p_z - q_z)^4}{R^2(p_\varphi - q_\varphi)^4}\right)}.$$

One can extract how the integral scales with q_φ or q_z by non dimensionalizing p_φ and p_z with either q_φ and q_φ^2 or $q_z^{1/2}$ and q_z respectively. By doing this one can find that the integral scales as $q_\varphi^{-1} \sim q_z^{-1/2}$. This observation tells us that the self consistent equation can be solved by the ansatz:

$$C_{\varphi\varphi\varphi\varphi}^R(\mathbf{q}) = q_\varphi^{\eta_\varphi} \Omega_{\varphi\varphi\varphi\varphi}(q_\varphi/(q_{\text{el}} q_z)^z). \tag{36}$$

Using simple power counting, we find that

$$\eta_\varphi = 1, z = 1/2. \tag{37}$$

From the form of the integral in Eq. 35, it is easy to see that the function $\Omega_{\varphi\varphi\varphi\varphi}$ is independent of q_φ when $q_\varphi \to 0$, as well as independent of q_z when $q_z \to 0$. This means the following:

$$\Omega_{\varphi\varphi\varphi\varphi}(x) \propto \begin{cases} \text{consant}, & x \to \infty \\ x^{-\eta_\varphi}, & x \to 0 \end{cases}. \tag{38}$$

This implies the following:

$$C_{\varphi\varphi\varphi\varphi}^R(\mathbf{q}) \propto \begin{cases} q_\varphi, & q < q_{\text{el}} < q_{\text{th}} \text{ and } q_\varphi \gg (q_{\text{el}} q_z)^{1/2} \\ \sqrt{q_z}, & q < q_{\text{el}} < q_{\text{th}} \text{ and } q_\varphi \ll (q_{\text{el}} q_z)^{1/2} \end{cases}. \tag{39}$$

Although the other moduli are irrelevant, we can repeat this same analysis to obtain how they scale. We can check how these moduli scale in our simulations and therefore better verify our theory and provide an understanding of the mechanical properties of nanotubes. We can check for example how the shear modulus should scale:

$$C_{\varphi z \varphi z}^R(\mathbf{q}) = C_{\varphi z \varphi z}^R(q_{\text{el}}) - \frac{k_B T}{2\pi^2} C_{\varphi z \varphi z}^R(\mathbf{q}) C_{\varphi z \varphi z}^R(q_{\text{el}}) \int dp_\varphi dp_z (p_\varphi - q_\varphi)(p_z - q_z) p_\varphi p_z \times$$

$$\frac{1}{\left(B_{\varphi\varphi\varphi\varphi}^R(q_{\text{el}}) p_\varphi^4 + \frac{Y_{zz}^R(q_{\text{el}}) p_z^4}{R^2 p_\varphi^4}\right) \left(B_{\varphi\varphi\varphi\varphi}^R(q_{\text{el}})(p_\varphi - q_\varphi)^4 + \frac{Y_{zz}^R(q_{\text{el}})(p_z - q_z)^4}{R^2(p_\varphi - q_\varphi)^4}\right)}. \tag{40}$$

By non dimensionalizing p_φ and p_z with either q_φ and q_φ^2 respectively, we find the integral scales as $q_\varphi \sim q_z^{1/2} \to 0$ as $q \to 0$. This implies that $C_{\varphi z \varphi z}^R(\mathbf{q}) \approx C_{\varphi z \varphi z}^R(q_{\text{el}})$:

$$C_{\varphi z \varphi z}^R(\mathbf{q}) \approx C_{\varphi z \varphi z}^R(q_{\text{el}}), \ q < q_{\text{el}} < q_{\text{th}}. \tag{41}$$
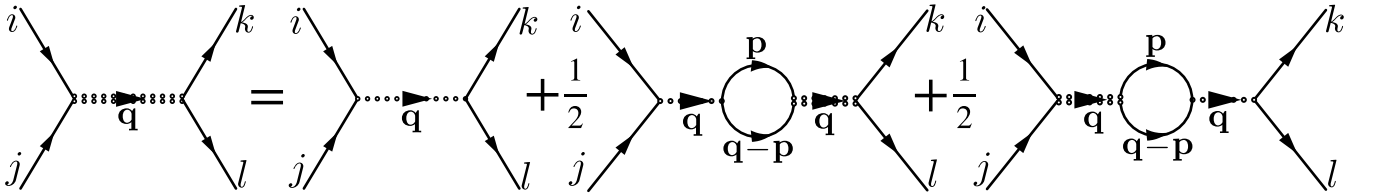

FIG. 4. The self consistent perturbative equation for $C_{ijkl}^R(\mathbf{q})$ is shown diagrammatically using the $C_{ijkl}\partial_i \tilde{h} \partial_j \tilde{h} \partial_k \tilde{h} \partial_l \tilde{h}$ vertex. The symmetrization is due to the major symmetry of the Hamiltonian. The dotted line indicates $C_{ijkl}^R(q_{\text{el}})$ and the doubled dotted line $C_{ijkl}^R(\mathbf{q})$.

Similarly, for $C_{\varphi\varphi zz}^R(\mathbf{q})$, we have the following self-consistent equation:

$$
\begin{aligned}
C_{\varphi\varphi zz}^R(\mathbf{q}) =& C_{\varphi\varphi zz}^R(q_{\text{el}}) \\
& - \frac{k_B T}{16\pi^2} \int dp_\varphi dp_z \frac{[C_{\varphi\varphi\varphi\varphi}^R(\mathbf{q})(p_\varphi - q_\varphi)^2 + C_{\varphi\varphi zz}^R(\mathbf{q})(p_z - q_z)^2][C_{\varphi\varphi zz}^R(q_{\text{el}})p_\varphi^2 + C_{zzzz}^R(q_{\text{el}})p_z^2]}{\left(B_{\varphi\varphi\varphi\varphi}^R(q_{\text{el}})p_\varphi^4 + \frac{Y_{zz}^R(q_{\text{el}})p_z^4}{R^2 p_\varphi^4}\right)\left(B_{\varphi\varphi\varphi\varphi}^R(q_{\text{el}})(p_\varphi - q_\varphi)^4 + \frac{Y_{zz}^R(q_{\text{el}})(p_z - q_z)^4}{R^2(p_\varphi - q_\varphi)^4}\right)} \\
& - \frac{k_B T}{16\pi^2} \int dp_\varphi dp_z \frac{[C_{\varphi\varphi\varphi\varphi}^R(q_{\text{el}})(p_\varphi - q_\varphi)^2 + C_{\varphi\varphi zz}^R(q_{\text{el}})(p_z - q_z)^2][C_{\varphi\varphi zz}^R(\mathbf{q})p_\varphi^2 + C_{zzzz}^R(\mathbf{q})p_z^2]}{\left(B_{\varphi\varphi\varphi\varphi}^R(q_{\text{el}})p_\varphi^4 + \frac{Y_{zz}^R(q_{\text{el}})p_z^4}{R^2 p_\varphi^4}\right)\left(B_{\varphi\varphi\varphi\varphi}^R(q_{\text{el}})(p_\varphi - q_\varphi)^4 + \frac{Y_{zz}^R(q_{\text{el}})(p_z - q_z)^4}{R^2(p_\varphi - q_\varphi)^4}\right)}.
\end{aligned}
\tag{42}
$$

Since the $C_{zzzz}^R(\mathbf{q})$ term is less relevant (has a lower scaling dimension) than the $C_{\varphi\varphi zz}^R(\mathbf{q})$ term, we may ignore its contribution to the equation. In addition $C_{zzzz}^R(q_{\text{el}})p_z^2$ scales with a higher power of q_φ than $C_{\varphi\varphi zz}(q_{\text{el}})p_z^2$ and may thus be ignored. The integral with coefficient $C_{\varphi\varphi\varphi\varphi}^R(\mathbf{q})C_{\varphi\varphi zz}^R(q_{\text{el}})$ scales as q_φ^{-1} and the integral with coefficient $C_{\varphi\varphi zz}^R(\mathbf{q})C_{\varphi\varphi zz}^R(q_{\text{el}})$ scales as q_φ. Finally, the integral with coefficient $C_{\varphi\varphi\varphi\varphi}(q_{\text{el}})C_{\varphi\varphi zz}^R(\mathbf{q})$ scales as q_φ^{-1}. In addition, as we have seen before, $C_{\varphi\varphi\varphi\varphi}^R(\mathbf{q}) \sim q_\varphi$. This means that the self consistent equation gives the following:

$$
\begin{aligned}
& C_{\varphi\varphi zz}^R(\mathbf{q}) \approx \text{const.} \times C_{\varphi\varphi zz}^R(q_{\text{el}}) + (\text{const.} \times q_\varphi + \text{const.} \times q_\varphi^{-1}) \times C_{\varphi\varphi zz}^R(\mathbf{q}), \ q < q_{\text{el}} < q_{\text{th}}, \\
& \Rightarrow C_{\varphi\varphi zz}^R(\mathbf{q})(1 + (\text{const.} \times q_\varphi + \text{const.} \times q_\varphi^{-1})) = \text{const.} \times C_{\varphi\varphi zz}^R(q_{\text{el}}), \ q < q_{\text{el}} < q_{\text{th}}.
\end{aligned}
\tag{43}
$$

Hence, for the two sides in the above equation to have the same scaling as $q_\varphi \to 0$, it is necessary that $C_{\varphi\varphi zz}^R(\mathbf{q}) \sim q_\varphi$ and thus more explicitly:

$$
C_{\varphi\varphi zz}^R(\mathbf{q}) \propto \begin{cases} q_\varphi, & q < q_{\text{el}} < q_{\text{th}} \text{ and } q_\varphi \gg (q_{\text{el}} q_z)^{1/2} \\ \sqrt{q_z}, & q < q_{\text{el}} < q_{\text{th}} \text{ and } q_\varphi \ll (q_{\text{el}} q_z)^{1/2} \end{cases}.
\tag{44}
$$

For $C_{zzzz}^R(\mathbf{q})$, we have the following self-consistent equation:

$$
\begin{aligned}
C_{zzzz}^R(\mathbf{q}) =& C_{zzzz}^R(q_{\text{el}}) - \frac{k_B T}{8\pi^2} \int dp_\varphi dp_z \\
& [C_{zzzz}^R(\mathbf{q})(p_z - q_z)q_z + C_{\varphi\varphi zz}^R(\mathbf{q})(p_\varphi - q_\varphi)q_\varphi][C_{zzzz}^R(q_{\text{el}})(p_z - q_z)q_z + C_{\varphi\varphi zz}^R(q_{\text{el}})(p_\varphi - q_\varphi)q_\varphi] \times \\
& \frac{1}{\left(B_{\varphi\varphi\varphi\varphi}^R(q_{\text{el}})p_\varphi^4 + \frac{Y_{zz}^R(q_{\text{el}})p_z^4}{R^2 p_\varphi^4}\right)\left(B_{\varphi\varphi\varphi\varphi}^R(q_{\text{el}})(p_\varphi - q_\varphi)^4 + \frac{Y_{zz}^R(q_{\text{el}})(p_z - q_z)^4}{R^2(p_\varphi - q_\varphi)^4}\right)}.
\end{aligned}
\tag{45}
$$

By non dimensionalizing p_φ and p_z with q_φ and q_φ^2 respectively, we find the integral scales as $q_\varphi^3 \sim q_z^{3/2} \to 0$ as $q_\varphi \to 0$. This implies that in the limit of $q_\varphi \to 0$, $C_{zzzz}^R(\mathbf{q}) \approx C_{zzzz}^R(q_{\text{el}})$:

$$
C_{zzzz}^R(\mathbf{q}) \approx C_{zzzz}^R(q_{\text{el}}), \ q < q_{\text{el}} < q_{\text{th}}.
\tag{46}
$$

Earlier, we found that $Y_{zz}^R(\mathbf{q})$ stops renormalizing in the regime $q < q_{\text{el}} < q_{\text{th}}$. But we know that $Y_{zz} = C_{zzzz} - C_{\varphi\varphi zz}^2/C_{\varphi\varphi\varphi\varphi}$. Since $C_{zzzz}^R \sim$ constant and $(C_{\varphi\varphi zz}^R)^2/C_{\varphi\varphi\varphi\varphi}^R \sim q_\varphi^2/q_\varphi = q_\varphi \to 0$ as $q_\varphi \to 0$, and therefore $C_{zzzz}^R - (C_{\varphi\varphi zz}^R)^2/C_{\varphi\varphi\varphi\varphi}^R \sim$ constant which matches with our result for Y_{zz}^R. Similarly, $Y_{\varphi\varphi} = C_{\varphi\varphi\varphi\varphi} - C_{\varphi\varphi zz}^2/C_{zzzz} \sim q_\varphi$. We summarize these scalings in Table I.

In the beginning of this section, we assumed $\ell_{\text{el}} \gg \ell_{\text{th}}$. However, even if $\ell_{\text{th}} > \ell_{el}$, all the analysis starting from the naïve dimensions in Eqs. 28 and 31 would remain the same in the regime $\ell > \ell_{\text{th}} > \ell_{el}$ except the fact that we would our starting course-grained free energy would be $F_{\text{eff}}(q_{\text{th}})$ instead of $F_{\text{eff}}(q_{\text{el}})$ in Eq. 24 and the material parameters in the course-grained free energy $F_{\text{eff}}(q_{\text{th}})$ would be $B_{ijkl}^R(q_{\text{th}}) \approx B_{ijkl}^0 = \kappa_0 \delta_{ij}\delta_{kl}$ and $C_{ijkl}^R(q_{\text{th}}) \approx C_{ijkl}^0 = \lambda_0 \delta_{ij}\delta_{kl} + \mu_0(\delta_{ik}\delta_{jl} + \delta_{il}\delta_{jk})$ instead of $B_{ijkl}^R(q_{\text{el}})$ and $C_{ijkl}^R(q_{\text{el}})$ in $F_{\text{eff}}(q_{\text{el}})$ since the elastic moduli do not renormalize in the regime $q > q_{\text{th}}$. We summarize these scalings in Table II.

Note that the scaling exponents in the regime $q < \min\{q_{\text{th}}, q_{\text{el}}\}$ hold to all orders of perturbation theory. This is because of the following reason. Since the parameters in the radial correlation function remain constant due to the irrelevance of all anharmonic terms in the effective free enegy F_{eff}, the scaling exponents of the in-plane moduli are obtained using simple power counting from self-consistent equations like Eqs. 35 and 45. This remains the same to all orders in perturbation [52].

TABLE I. Scaling functions for $\ell_{\mathrm{th}} < \ell_{\mathrm{el}} \Rightarrow q_{\mathrm{th}} > q_{\mathrm{el}}$

Scale	$q > q_{\mathrm{th}} > q_{\mathrm{el}}$	$q_{\mathrm{th}} > q > q_{\mathrm{el}}$	$q_{\mathrm{th}} > q_{\mathrm{el}} > q$
$C^R_{\varphi\varphi\varphi\varphi}/Y_0$	$\frac{1}{1-\nu_0^2}$	$\left(\frac{q}{q_{\mathrm{th}}}\right)^{\eta_u}$	$\left(\frac{q_{\mathrm{el}}}{q_{\mathrm{th}}}\right)^{\eta_u}\left(\frac{q_\varphi}{q_{\mathrm{el}}}\right)\Omega_{\varphi\varphi\varphi\varphi}\left(q_\varphi/(q_{\mathrm{el}}q_z)^{1/2}\right)$
$C^R_{\varphi\varphi zz}/Y_0$	$\frac{\nu_0}{1-\nu_0^2}$	$\left(\frac{q}{q_{\mathrm{th}}}\right)^{\eta_u}$	$\left(\frac{q_{\mathrm{el}}}{q_{\mathrm{th}}}\right)^{\eta_u}\left(\frac{q_\varphi}{q_{\mathrm{el}}}\right)\Omega_{\varphi\varphi zz}\left(q_\varphi/(q_{\mathrm{el}}q_z)^{1/2}\right)$
$C^R_{\varphi z\varphi z}/Y_0$	$\frac{1}{2(1+\nu_0)}$	$\left(\frac{q}{q_{\mathrm{th}}}\right)^{\eta_u}$	$\left(\frac{q_{\mathrm{el}}}{q_{\mathrm{th}}}\right)^{\eta_u}$
C^R_{zzzz}/Y_0	$\frac{1}{1-\nu_0^2}$	$\left(\frac{q}{q_{\mathrm{th}}}\right)^{\eta_u}$	$\left(\frac{q_{\mathrm{el}}}{q_{\mathrm{th}}}\right)^{\eta_u}$
$Y^R_{\varphi\varphi}/Y_0$	1	$\left(\frac{q}{q_{\mathrm{th}}}\right)^{\eta_u}$	$\left(\frac{q_{\mathrm{el}}}{q_{\mathrm{th}}}\right)^{\eta_u}\left(\frac{q_\varphi}{q_{\mathrm{el}}}\right)\Omega_{Y_{\varphi\varphi}}\left(q_\varphi/(q_{\mathrm{el}}q_z)^{1/2}\right)$
Y^R_{zz}/Y_0	1	$\left(\frac{q}{q_{\mathrm{th}}}\right)^{\eta_u}$	$\left(\frac{q_{\mathrm{el}}}{q_{\mathrm{th}}}\right)^{\eta_u}$
$B^R_{\varphi\varphi\varphi}/\kappa_0$	1	$\left(\frac{q}{q_{\mathrm{th}}}\right)^{-\eta}$	$\left(\frac{q_{\mathrm{el}}}{q_{\mathrm{th}}}\right)^{-\eta}$

TABLE II. Scaling Exponents for $\ell_{\mathrm{el}} < \ell_{\mathrm{th}} \Rightarrow q_{\mathrm{el}} > q_{\mathrm{th}}$

Scale	$q > q_{\mathrm{el}} > q_{\mathrm{th}}$	$q_{\mathrm{el}} > q > q_{\mathrm{th}}$	$q_{\mathrm{el}} > q_{\mathrm{th}} > q$
$C^R_{\varphi\varphi\varphi\varphi}/Y_0$	$\frac{1}{1-\nu_0^2}$	$\frac{1}{1-\nu_0^2}$	$\sim \left(\frac{q_\varphi}{q_{\mathrm{el}}}\right)\Omega_{\varphi\varphi\varphi\varphi}\left(q_\varphi/(q_{\mathrm{el}}q_z)^{1/2}\right)$
$C^R_{\varphi\varphi zz}/Y_0$	$\frac{\nu_0}{1-\nu_0^2}$	$\frac{\nu_0}{1-\nu_0^2}$	$\sim \left(\frac{q_\varphi}{q_{\mathrm{el}}}\right)\Omega_{\varphi\varphi zz}\left(q_\varphi/(q_{\mathrm{el}}q_z)^{1/2}\right)$
$C^R_{\varphi z\varphi z}/Y_0$	$\frac{1}{2(1+\nu_0)}$	$\frac{1}{2(1+\nu_0)}$	constant
C^R_{zzzz}/Y_0	$\frac{1}{1-\nu_0^2}$	$\frac{1}{1-\nu_0^2}$	constant
$Y^R_{\varphi\varphi}/Y_0$	1	1	$\sim \left(\frac{q_\varphi}{q_{\mathrm{el}}}\right)\Omega_{Y_{\varphi\varphi}}\left(q_\varphi/(q_{\mathrm{el}}q_z)^{1/2}\right)$
Y^R_{zz}/Y_0	1	1	constant
$B^R_{\varphi\varphi\varphi}/\kappa_0$	1	1	constant

V.   COMPARISON WITH MOLECULAR DYNAMICS SIMULATIONS

To test our results tabulated in Tables I and II, we compared with molecular dynamics (MD) simulations. Instead of using a fully atomistic model to simulate a nanotube, we used a convenient coarse-grained discrete model made of a triangular lattice of point masses with nearest neighbors connected by harmonic springs (see Fig. 1(a)). Then the stretching part in the free energy in Eq. 3 can be modeled by assigning the equilibrium length of the springs to be a_0 and a spring constant K_b:

$$F_{\mathrm{stretch}} = \frac{1}{2}K_b \sum_{\langle i,j\rangle}(|\mathbf{x}_i - \mathbf{x}_j| - a_0)^2, \tag{47}$$

where $\mathbf{x}_i$ is the position of ith mass and the sum is over nearest neighbor point masses i and j. The energy cost of bending in Eq. 3 can be modeled as [33, 55]:

$$F_{\mathrm{bending}} = K_d \sum_{(\alpha,\beta)}(1 + \cos(\theta_{\alpha\beta} - \theta^0_{\alpha\beta})), \tag{48}$$

where $\theta_{\alpha\beta}$ is the angle between two adjacent triangles α and β as shown in Fig. 1(a) and $\theta^0_{\alpha\beta}$ is the value of this angle at minimum bending energy configuration. Note that $\theta^0_{\alpha\beta}$ depends on the curvature of the nanotube and fineness of the discretization. The parameters K_b and K_d are related to the continuum material parameters as follows [55]:

$$Y_0 = \frac{2}{\sqrt{3}}K_b, \lambda_0 = \mu_0 = \frac{\sqrt{3}}{4}K_b, \nu_0 = \frac{1}{3}, \kappa_0 = \frac{\sqrt{3}}{2}K_d. \tag{49}$$

The simulations were done with LAMMPS package [56, 57]. As will be discussed later, the simulations were done in isobaric-isothermal (NPT) or canonical (NVT) ensemble. Temperature and pressure were controlled using Nosé-Hoover type thermostat and barostat [58]. The parameters K_d, K_b, T, the aspect ratio $L/(2\pi R)$ and number of point masses were varied to probe different scaling regimes. The time steps were chosen to be one tenth of the smallest of the characteristic time scales of the system:

$$\tau_T = a\sqrt{\frac{m}{k_B T}}, \tau_b = \sqrt{\frac{m}{K_b}}, \tau_d = a_0\sqrt{\frac{m}{K_d}}, \tag{50}$$

where m is the mass of each point mass, and τ_T is characteristic time a point mass takes to cover one atomic length at thermal velocity, τ_b is characteristic time of the spring-mass system, τ_d is characteristic time of the dihedral bond-mass system. A simulation generally ran for approximately $1.6\mathrm{x}10^8 - 10^9$ time steps. For each simulation, the equilibration was checked using autocorrelation time of different parameters such as radial fluctuations, length of the shell, etc.

First, simulations were done with periodic boundary condition along the axial direction and the simulation box was allowed to change its size in the axial direction maintaining zero pressure condition so that the cylindrical shell could fluctuate freely. From these simulations, the radial displacements were calculated. The Fourier transform of the correlation function $\langle|\tilde{h}(q_\varphi, q_z = 0)|^2\rangle$ and $\langle|\tilde{h}(q_\varphi = 0, q_z)|^2\rangle$ of radial displacement are plotted in Fig. 5. Fig. 5(a) shows the collapse around q_{th}. The dotted lines for $\langle|\tilde{h}(q_\varphi, q_z = 0)|^2\rangle$ and $\langle|\tilde{h}(q_\varphi = 0, q_z)|^2\rangle$ coincide with each other in the region $q > q_{\mathrm{el}}$ for each parameter set. This is because in this regime the effect of anisotropic curvature is negligible in this regime. Furthermore, in this regime, we see that the correlation function goes as $\sim q^{-4}$ when $q > q_{\mathrm{th}}$ and $\sim q^{-3.2}$ when $q < q_{\mathrm{th}}$. This is because in the former case the effect of the anharmonic terms are not important and the system is in the harmonic regime, whereas in the latter case the anharmonic terms are important and since $q > q_{\mathrm{el}}$ we see the exponent $-4 + \eta = -3.2$. However, in the regime $q < q_{\mathrm{el}}$ they diverge from each other. To understand this regime better, scaling collapse around q_{el} is done in Fig. 5(b) keeping $q_{\mathrm{el}} \leq q_{\mathrm{th}}$ for all simulations. Again, for $q > q_{\mathrm{el}}$, $\langle|\tilde{h}(q_\varphi, q_z = 0)|^2\rangle$ and $\langle|\tilde{h}(q_\varphi = 0, q_z)|^2\rangle$ coincide with each other and scale as $\sim q^{-3.2}$ because here $q_{\mathrm{el}} < q < q_{\mathrm{th}}$. However, for $q < q_{\mathrm{el}} < q_{\mathrm{th}}$, we see new scaling laws. In the φ direction the correlation function scales as $\sim q_\varphi^{-4}$, whereas in the z direction the correlation function scales as $\sim q_z^{-1/2}$. These observations can be justified using the Green's function in Eq. 11 and Table I in the following way:

$$\langle|\tilde{h}(q_\varphi, q_z = 0)|^2\rangle = \frac{k_B T/A}{B^R_{\varphi\varphi\varphi\varphi}(\mathbf{q})q_\varphi^4} = \frac{k_B T/A}{\kappa_R(\mathbf{q})q_\varphi^4} \approx \frac{k_B T/A}{\kappa_0(q_{\mathrm{el}}/q_{\mathrm{th}})^{-\eta}q_\varphi^4} \text{ for } q_\varphi < q_{\mathrm{el}} < q_{\mathrm{th}}, \tag{51a}$$

$$\langle|\tilde{h}(q_\varphi = 0, q_z)|^2\rangle = \frac{k_B T/A}{B^R_{zzzz}(\mathbf{q})q_z^4 + \frac{Y^R_{\varphi\varphi}(\mathbf{q})}{R^2}} \approx \frac{k_B T/A}{Y^R_{\varphi\varphi}(\mathbf{q})/R^2} \approx \frac{k_B T/A}{Y_0(q_{\mathrm{el}}/q_{\mathrm{th}})^{\eta_u}(q_z/q_{\mathrm{el}})^{1/2}/R^2} \text{ for } q_z < q_{\mathrm{el}} < q_{\mathrm{th}}. \tag{51b}$$

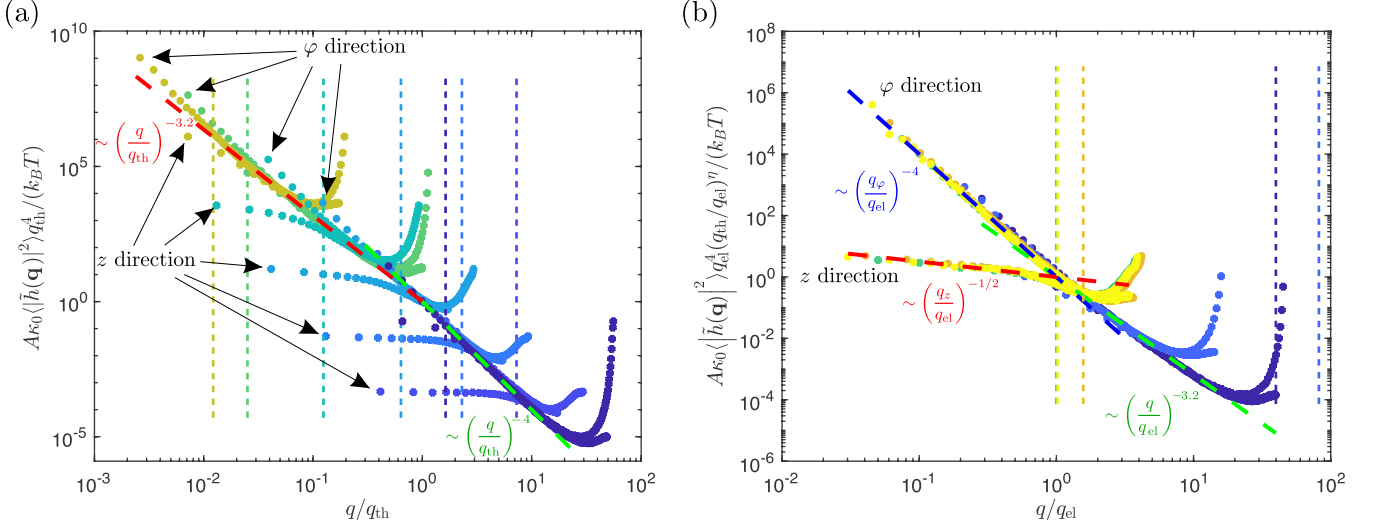In total, both panels of Fig. 5 can be summarized using the following equations:

FIG. 5. Scaling collapse for radial displacement correlation function $\langle|\tilde{h}(\mathbf{q})|^2\rangle$ for molecular dynamics simulations with zero pressure condition in the axial direction. (a) Correlation function $\langle|\tilde{h}(q_\varphi, q_z = 0)|^2\rangle$ and $\langle|\tilde{h}(q_\varphi = 0, q_z)|^2\rangle$ collapsed around q_{th} plotted in dots. For a single parameter set, the same color was used to plot the correlation function in both φ and z direction. The dotted lines of different colors correspond to different parameter sets. The vertical dashed lines of different colors show $q_{\mathrm{el}}/q_{\mathrm{th}}$ corresponding to the dotted curves of same color. The red and green slanted dashed lines are $(q_\varphi/q_{\mathrm{th}})^{-3.2}$ and $(q_\varphi/q_{\mathrm{th}})^{-4}$ respectively. (b) Correlation functions $\langle|\tilde{h}(q_\varphi, q_z = 0)|^2\rangle$ and $\langle|\tilde{h}(q_\varphi = 0, q_z)|^2\rangle$ collapsed around q_{el} plotted in dots. For a single parameter set, the same color was used to plot the correlation function in both φ and z direction. The vertical dashed lines of different colors show q_{th}/q_{el} corresponding to the dotted curves of same color. The red, blue and green slanted dashed lines are $(q_z/q_{\mathrm{th}})^{-1/2}$, $(q_\varphi/q_{\mathrm{th}})^{-1/2}$ and $(q/q_{\mathrm{th}})^{-3.2}$ respectively. In both panels, the curling up of the tails of the simulation curves corresponds to wave vectors close to the edge of the first Brillouin zone.

$$\langle|\tilde{h}(q_\varphi, q_z=0)|^2\rangle = \frac{k_B T/A}{B^R_{\varphi\varphi\varphi}(\mathbf{q})q_\varphi^4} \approx \begin{cases} \frac{k_B T/A}{\kappa_0 q_\varphi^4}, & q_{\mathrm{el}} < q_{\mathrm{th}} < q_\varphi \\ \frac{k_B T/A}{\kappa_0 (q_\varphi/q_{\mathrm{th}})^{-\eta}q_\varphi^4}, & q_{\mathrm{el}} < q_\varphi < q_{\mathrm{th}} \\ \frac{k_B T/A}{\kappa_0 (q_{\mathrm{el}}/q_{\mathrm{th}})^{-\eta}q_\varphi^4}, & q_\varphi < q_{\mathrm{el}} < q_{\mathrm{th}} \end{cases} \tag{52a}$$

$$\langle|\tilde{h}(q_\varphi=0, q_z)|^2\rangle = \frac{k_B T/A}{B^R_{zzzz}(\mathbf{q})q_z^4 + \frac{Y^R_{\varphi\varphi}(\mathbf{q})}{R^2}} \approx \begin{cases} \frac{k_B T/A}{\kappa_R(\mathbf{q})q_z^4}, & q_{\mathrm{el}} < q_z \\ \frac{k_B T/A}{Y^R_{\varphi\varphi}(\mathbf{q})/R^2}, & q_z < q_{\mathrm{el}} \end{cases} \approx \begin{cases} \frac{k_B T/A}{\kappa_0 q_z^4}, & q_{\mathrm{el}} < q_{\mathrm{th}} < q_z \\ \frac{k_B T/A}{\kappa_0 (q_z/q_{\mathrm{el}})^{-\eta}q_z^4}, & q_{\mathrm{el}} < q_z < q_{\mathrm{th}} \\ \frac{k_B T/A}{Y_0 (q_{\mathrm{el}}/q_{\mathrm{th}})^{\eta_u}(q_z/q_{\mathrm{el}})^{1/2}/R^2}, & q_z < q_{\mathrm{el}} < q_{\mathrm{th}} \end{cases} \tag{52b}$$

This confirms the nontrivial scaling of $Y_{\varphi\varphi}$ in the regime $q < q_{\mathrm{el}} < q_{\mathrm{th}}$ as we predicted in Section IV B.

To probe the Young's modulus Y_{zz} in the axial direction, we performed simulations changing the length of the box in steps and at each step letting the shell equilibrate under thermal fluctuation. This ensemble is canonical (NVT) since we fixed the volume of the system at each step. Then, at each value of box length we recorded the pressure of the box in the axial direction. From that, we extracted the normal stress in the axial direction σ_{zz} (to get the stress from the pressure, we multiply the pressure with the area of the wall and divide by the perimeter of the nanotube) and plotted the average value of that as a function of strain (defined as the relative change of length from the size of the box at the minimum energy configuration) for different values of temperature T in Fig. 6(a). Note that in the figure, the strain at which the average stress is zero is different for different temperatures. This is because under thermal fluctuations, the shell shrinks (see Eq. 8b) in equilibrium (at zero external stress condition on the average). More
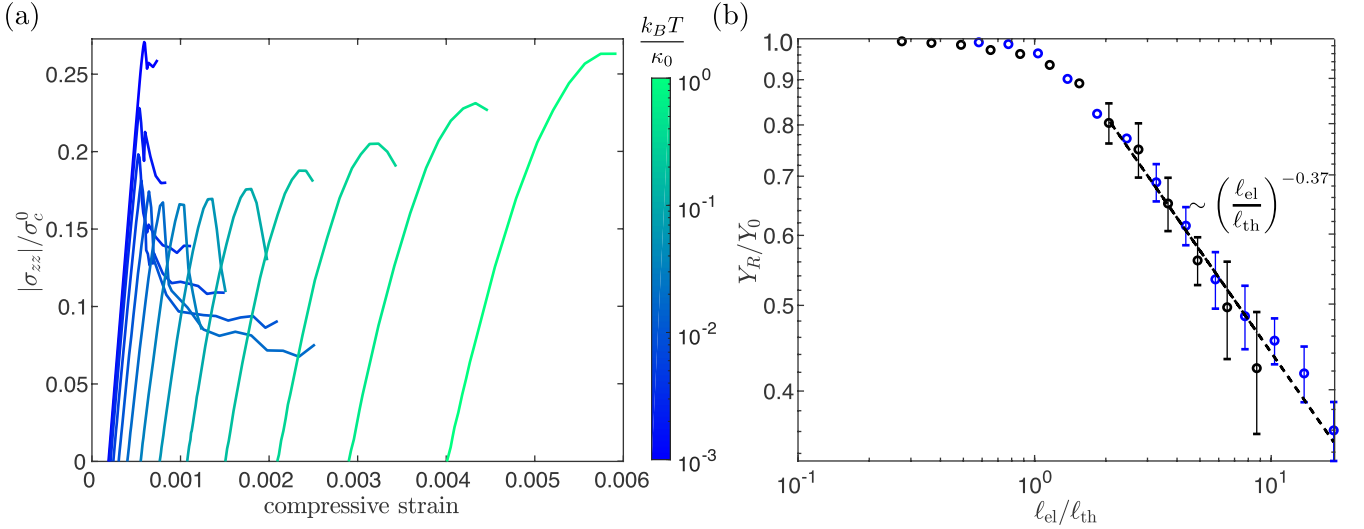

FIG. 6. Simulation results from NVT simulations fixing the length of the cylindrical shell. (a) Stress vs. strain curves for a fixed parameter set $\gamma = 2 \times 10^6$, $L/2\pi R = 2$, $2\pi R/a_0 = 48$ at different temperatures (the colorbar shows k_B/κ_0). The vertical axis of the plot is $|\sigma_{zz}|/\sigma_c^0$, where $\sigma_c^0 = 2\sqrt{Y_0\kappa_0}/R$ is the critical buckling load for classical cylindrical shell [59]. The maximum of the curve at each temperature is the critical buckling load for molecular dynamics, which is smaller than the classical buckling load σ_c^0 because of the discrete nature and corresponding non-ideality of our model. (b) Young's modulus extracted from the slope of the strain vs. strain curves (example shown in (a)) at zero stress plotted as a function of $\ell_{\mathrm{el}}/\ell_{\mathrm{th}}$. The black dots correspond to the parameter set $\gamma = Y_0 R^2/\kappa_0 = 1 \times 10^5$, $L/2\pi R = 1$, $2\pi R/a_0 = 48$, $L/\ell_{\mathrm{el}} \approx 35$. The blue dots correspond to the parameter set $\gamma = Y_0 R^2/\kappa_0 = 2 \times 10^6$, $L/2\pi R = 2$, $2\pi R/a_0 = 48$, $L/\ell_{\mathrm{el}} \approx 126$. The black dashed line shows $(\ell_{\mathrm{el}}/\ell_{\mathrm{th}})^{-0.37}$.

importantly, we notice that the slope of the stress vs. strain curves change with temperature. The slope of the stress vs. strain curve at zero stress is defined as the Young's modulus Y_{zz} in the axial direction. We plotted the normalized Young's modulus Y_{zz}/Y_0, extracted this way, as a function of $\ell_{\mathrm{el}}/\ell_{\mathrm{th}}$ in Fig. 6(b) for two different parameter sets. The Young's moduli for these two parameter sets decrease with increasing system size but only collapse on top of each other when the horizontal axis is $\ell_{\mathrm{el}}/\ell_{\mathrm{th}}$ in fig. 6(b). This implies that Y_{zz} stops renormalizing at the elastic length scale ℓ_{el} confirming Eq. 34b. Furthermore, from Fig. 6(b), we see that the Y^R_{zz} scales as $\sim (\ell_{\mathrm{el}}/\ell_{\mathrm{th}})^{-0.37} = (\ell_{\mathrm{el}}/\ell_{\mathrm{th}})^{-\eta_u}$ confirming the scaling law in the regime $\ell_{\mathrm{th}} < \ell < \ell_{\mathrm{el}}$.

VI. CONCLUSION

We have studied the mechanical properties of thermally fluctuating nanotubes. We have shown that the presence of length scales ℓ_{th} and ℓ_{el} gives different scaling regimes. In particular, at scales larger than both ℓ_{th} and ℓ_{el}, we find that the moduli become anisotropic. Moreover, in this regime, we obtain new scaling exponents for the elastic moduli. For system sizes falling between these two lenth scales and with $\ell_{th} < \ell_{el}$, we recover the same scaling exponents as in the case of isotropic flat solid membranes. We also note that these scaling results have been obtained previously in tubules [52] as well as membranes under uni-axial tension [54]. It would be of interest to find other physical scenarios that exhibit similar scaling behaviors.

One immediate extension of this work can be to study the effect of thermal fluctuations on the critical axial buckling load. We see from Fig. 6(a), the critical buckling load initially reduces with increasing temperature (see the bluer curves), but starts increasing (see the greener curves) with increasing temperature. We anticipate that the initial dip is due to the thermal activation over the energy barrier crossing to the buckled state, but the later increase is due to renormalization of elastic moduli. However, deeper investigation is required for better understanding.

The theory presented here is limited to shells with length L to circumference $2\pi R$ with a ratio of order 1. However, shells with $L \gg 2\pi R$ or $L \ll 2\pi R$ may also be importance. In both cases, one can, in principle, integrate out the Fourier modes in the shorter direction and study the effectively 1-dimensional system. In the case $L \gg 2\pi R$, we expect the shell to behave like a polymer chain [60] and perform a random walk when the length is larger than its persistence length. In the case $L \ll 2\pi R$, we expect the shell to behave like an elastic ring which also performs a random walk beyond a persistence length [61] and can show interesting instabilities under axisymmetric pressure [62].

While the results presented here are for single-walled nanotubes, similar studies can also be done with multi-walled nanotubes. Whereas a realistic model with van der Waals interactions between layers may be too difficult for analytical methods, a phenomenological elasticity-like model as described in [63] adapted for cylindrical shells may be more amenable to analytical studies.

[1] K. S. Novoselov, D. Jiang, F. Schedin, T. Booth, V. Khotkevich, S. Morozov, and A. K. Geim, "Two-dimensional atomic crystals," *Proceedings of the National Academy of Sciences*, vol. 102, no. 30, pp. 10451–10453, 2005.

[2] S. Iijima, "Helical microtubules of graphitic carbon," *Nature*, vol. 354, pp. 56–58, 1991.

[3] D. Lembke, S. Bertolazzi, and A. Kis, "Single-layer mos2 electronics," *Accounts of Chemical Research*, vol. 48, no. 1, pp. 100–110, 2015.

[4] G. Bhimanapati, N. Glavin, and J. Robinson, "Chapter three - 2d boron nitride: Synthesis and applications," in *2D Materials* (F. Iacopi, J. J. Boeckl, and C. Jagadish, eds.), vol. 95 of *Semiconductors and Semimetals*, pp. 101–147, Elsevier, 2016.

[5] L. Joly-Pottuz and M. Iwaki, "14 - superlubricity of tungsten disulfide coatings in ultra high vacuum," in *Superlubricity* (A. Erdemir and J.-M. Martin, eds.), pp. 227–236, Amsterdam: Elsevier Science B.V., 2007.

[6] C. Gao, E. Donath, S. Moya, V. Dudnik, and H. Möhwald, "Elasticity of hollow polyelectrolyte capsules prepared by the layer-by-layer technique," *The European Physical Journal E*, vol. 5, pp. 21–28, 2001.

[7] V. D. Gordon, X. Chen, J. W. Hutchinson, A. R. Bausch, M. Marquez, and D. A. Weitz, "Self-assembled polymer membrane capsules inflated by osmotic pressure," *Journal of the American Chemical Society*, vol. 126, no. 43, pp. 14117–14122, 2004.

[8] V. V. Lulevich, D. Andrienko, and O. I. Vinogradova, "Elasticity of polyelectrolyte multilayer microcapsules," *The Journal of Chemical Physics*, vol. 120, no. 8, pp. 3822–3826, 2004.

[9] J. Lidmar, L. Mirny, and D. R. Nelson, "Virus shapes and buckling transitions in spherical shells," *Phys. Rev. E*, vol. 68, p. 051910, Nov 2003.

[10] I. L. Ivanovska, P. J. de Pablo, B. Ibarra, G. Sgalari, F. C. MacKintosh, J. L. Carrascosa, C. F. Schmidt, and G. J. L. Wuite, "Bacteriophage capsids: Tough nanoshells with complex elastic properties," *Proceedings of the National Academy of Sciences*, vol. 101, no. 20, pp. 7600–7605, 2004.

[11] J. P. Michel, I. L. Ivanovska, M. M. Gibbons, W. S. Klug, C. M. Knobler, G. J. L. Wuite, and C. F. Schmidt, "Nanoindentation studies of full and empty viral capsids and the effects of capsid protein mutations on elasticity and strength," *Proceedings of the National Academy of Sciences*, vol. 103, no. 16, pp. 6184–6189, 2006.

[12] S. Wang, H. Arellano-Santoyo, P. A. Combs, and J. W. Shaevitz, "Actin-like cytoskeleton filaments contribute to cell mechanics in bacteria," *Proceedings of the National Academy of Sciences*, vol. 107, no. 20, pp. 9182–9185, 2010.

[13] D. R. Nelson, "Biophysical dynamics in disorderly environments," *Annual Review of Biophysics*, vol. 41, no. 1, pp. 371–402, 2012.

[14] A. Amir, F. Babaeipour, D. B. McIntosh, D. R. Nelson, and S. Jun, "Bending forces plastically deform growing bacterial cell walls," *Proceedings of the National Academy of Sciences*, vol. 111, no. 16, pp. 5778–5783, 2014.

[15] R. Waugh and E. Evans, "Thermoelasticity of red blood cell membrane," *Biophysical Journal*, vol. 26, no. 1, pp. 115–131, 1979.

[16] Y. Park, C. A. Best, K. Badizadegan, R. R. Dasari, M. S. Feld, T. Kuriabova, M. L. Henle, A. J. Levine, and G. Popescu,

"Measurement of red blood cell mechanics during morphological changes," *Proceedings of the National Academy of Sciences*, vol. 107, no. 15, pp. 6731–6736, 2010.

[17] E. Evans, "Bending elastic modulus of red blood cell membrane derived from buckling instability in micropipet aspiration tests," *Biophysical Journal*, vol. 43, no. 1, pp. 27–30, 1983.

[18] D. Nelson and L. Peliti, "Fluctuations in membranes with crystalline and hexatic order," *Journal de physique*, vol. 48, no. 7, pp. 1085–1092, 1987.

[19] Y. Kantor and D. R. Nelson, "Crumpling transition in polymerized membranes," *Physical review letters*, vol. 58, no. 26, p. 2774, 1987.

[20] M. Paczuski, M. Kardar, and D. R. Nelson, "Landau theory of the crumpling transition," *Phys. Rev. Lett.*, vol. 60, pp. 2638–2640, 1988.

[21] F. David and E. Guitter, "Crumpling transition in elastic membranes: Renormalization group treatment," *EPL*, vol. 5, no. 8, pp. 709–713, 1988.

[22] E. Guitter, F. David, S. Leibler, and L. Peliti, "Thermodynamical behavior of polymerized membranes," *Journal de Physique*, vol. 50, no. 14, pp. 1787–1819, 1989.

[23] J. Aronovitz, L. Golubovic, T. C. Lubensky, and L. Golubovi0107, "Fluctuations and lower critical dimensions of crystalline membranes fluctuations and lower critical dimensions of crystalline membranes," *Journal de Physique*, vol. 50, no. 6, pp. 609–631, 1989.

[24] J. A. Aronovitz and T. C. Lubensky, "Fluctuations of solid membranes," *Physical review letters*, vol. 60, no. 25, p. 2634, 1988.

[25] L. Radzihovsky and D. R. Nelson, "Statistical mechanics of randomly polymerized membranes," *Physical Review A*, vol. 44, no. 6, pp. 3525–3542, 1991.

[26] P. Le Doussal and L. Radzihovsky, "Self-consistent theory of polymerized membranes," *Phys. Rev. Lett.*, vol. 69, pp. 1209–1212, Aug 1992.

[27] P. Le Doussal and L. Radzihovsky, "Anomalous elasticity, fluctuations and disorder in elastic membranes," *Annals of Physics*, vol. 392, pp. 340–410, 2018.

[28] J.-P. Kownacki and D. Mouhanna, "Crumpling transition and flat phase of polymerized phantom membranes," *Phys. Rev. E*, vol. 79, p. 040101, 2009.

[29] F. L. Braghin and N. Hasselmann, "Thermal fluctuations of free-standing graphene," *Phys. Rev. B*, vol. 82, p. 035407, 2010.

[30] N. Hasselmann and F. L. Braghin, "Nonlocal effective-average-action approach to crystalline phantom membranes," *Phys. Rev. E*, vol. 83, p. 031137, 2011.

[31] A. Košmrlj and D. R. Nelson, "Thermal excitations of warped membranes," *Phys. Rev. E*, vol. 89, p. 022126, 2014.

[32] J. H. Los, A. Fasolino, and M. I. Katsnelson, "Scaling behavior and strain dependence of in-plane elastic properties of graphene," *Phys. Rev. Lett.*, vol. 116, p. 015901, 2016.

[33] M. J. Bowick, A. Košmrlj, D. R. Nelson, and R. Sknepnek, "Non-hookean statistical mechanics of clamped graphene ribbons," *Phys. Rev. B*, vol. 95, p. 104109, Mar 2017.

[34] A. Morshedifard, M. Ruiz-García, M. J. Abdolhosseini Qomi, and A. Košmrlj, "Buckling of thermalized elastic sheets," *Journal of the Mechanics and Physics of Solids*, vol. 149, p. 104296, 2021.

[35] G. López-Polín, C. Gómez-Navarro, V. Parente, F. Guinea, M. I. Katsnelson, F. Pérez-Murano, and J. Gómez-Herrero, "Increasing the elastic modulus of graphene by controlled defect creation," *Nature Physics*, vol. 11, pp. 26–31, 2015.

[36] T. Tombler, C. Zhou, L. Alexseyev, J. Kong, H. Dai, L. Liu, C. Jayanthi, M. Tang, and S.-Y. Wu, "Reversible electromechanical characteristics of carbon nanotubes under local-probe manipulation," *Nature*, vol. 405, no. 6788, pp. 769–772, 2000.

[37] M.-F. Yu, O. Lourie, M. J. Dyer, K. Moloni, T. F. Kelly, and R. S. Ruoff, "Strength and breaking mechanism of multiwalled carbon nanotubes under tensile load," *Science*, vol. 287, no. 5453, pp. 637–640, 2000.

[38] "Mechanical and thermal properties of carbon nanotubes," *Carbon*, vol. 33, no. 7, pp. 925–930, 1995.

[39] "Energy and environmental applications of carbon nanotubes," *Environmental Chemistry Letters*, vol. 10, no. 7, pp. 265–273, 2012.

[40] S. G. Noyce, J. L. Doherty, Z. Cheng, H. Han, S. Bowen, and A. D. Franklin, "Electronic stability of carbon nanotube transistors under long-term bias stress," *Nano Letters*, vol. 19, no. 3, pp. 1460–1466, 2019.

[41] V. A. Kobzev, N. G. Chechenin, K. A. Bukunov, E. A. Vorobyeva, and A. V. Makunin, "Structural and functional properties of composites with carbon nanotubes for space applications," *Materials Today: Proceedings*, vol. 5, no. 12, Part 3, pp. 26096–26103, 2018.

[42] J. L. Sanders, "Nonlinear theories for thin shells," *Quarterly of Applied Mathematics*, vol. 21, no. 1, pp. 21–36, 1963.

[43] L. H. Donnell, "Stability of thin-walled tubes under torsion," *NACA Technical Report 479*, 1933.

[44] K. Mushtari and K. Galimov, *Non-linear Theory of Thin Elastic Shells*. Israel program for scientific translations, 1961.

[45] A. Košmrlj and D. R. Nelson, "Statistical mechanics of thin spherical shells," *Phys. Rev. X*, vol. 7, p. 011002, Jan 2017.

[46] S. Komura and R. Lipowsky, "Fluctuations and stability of polymerized vesicles," *Journal de Physique II*, vol. 2, no. 8, pp. 1563–1575, 1992.

[47] In principle, a cylindrical shell should have different inner and outer radii since it can have finite thickness, for atomatically thin nanotubes thickness is not defined. However, as we will see later, an effective thickness can be defined in terms of its bending rigidity and in-plane moduli.

[48] M. Peskin, *An introduction to quantum field theory*. CRC press, 2018.

[49] A. Košmrlj and D. R. Nelson, "Response of thermalized ribbons to pulling and bending," *Phys. Rev. B*, vol. 93, p. 125431,

2016.

[50] D. Amit, *Field Theory, The Renormalization Group And Critical Phenomena (2nd Edition).* International series in pure and applied physics, World Scientific Publishing Company, 1984.

[51] H. Kleinert and V. Schulte-Frohlinde, *Critical Properties of ϕ^4-theories.* World Scientific, 2001.

[52] L. Radzihovsky and J. Toner, "Elasticity, shape fluctuations, and phase transitions in the new tubule phase of anisotropic tethered membranes," *Phys. Rev. E*, vol. 57, pp. 1832–1863, Feb 1998.

[53] H. W. Diehl and M. Shpot, "Critical behavior at m-axial lifshitz points: Field-theory analysis and ϵ-expansion results," *Phys. Rev. B*, vol. 62, pp. 12338–12349, 2000.

[54] M. E. H. Bahri, S. Sarkar, and A. Košmrlj, "Mechanical properties of fluctuating elastic membranes under uni-axial tension," *arXiv preprint arXiv:2209.09350*, 2022.

[55] H. S. Seung and D. R. Nelson, "Defects in flexible membranes with crystalline order," *Phys. Rev. A*, vol. 38, pp. 1005–1018, 1988.

[56] S. Plimpton, "Fast parallel algorithms for short-range molecular dynamics," *Journal of Computational Physics*, vol. 117, no. 1, pp. 1–19, 1995.

[57] http://lammps.sandia.gov. Accessed in November 2019.

[58] M. Tuckerman, *Statistical Mechanics: Theory and Molecular Simulation.* Oxford Graduate Texts, 2010.

[59] S. Timoshenko and J. Gere, *Theory of Elastic Stability.* Dover Civil and Mechanical Engineering, Dover Publications, 2012.

[60] P.-G. De Gennes and P.-G. Gennes, *Scaling concepts in polymer physics.* Cornell university press, 1979.

[61] Y. Rabin and S. Panyukov, "Thermal fluctuations of elastic ring," *arXiv preprint arXiv:cond-mat/0010488*, 2000.

[62] E. Katifori, S. Alben, and D. R. Nelson, "Collapse and folding of pressurized rings in two dimensions," *Phys. Rev. E*, vol. 79, p. 056604, May 2009.

[63] A. Mauri, D. Soriano, and M. I. Katsnelson, "Thermal ripples in bilayer graphene," *Phys. Rev. B*, vol. 102, p. 165421, Oct 2020.